Equivalent circuit modeling of InP/InGaAs Heterojunction Phototransistor for application of Radio-on-fiber systems

Jae-Young Kim

The Graduate School

Yonsei University

Department of Electrical and Electronic Engineering

Equivalent circuit modeling of InP/InGaAs Heterojunction Phototransistor for application of Radio-on-fiber systems

Master's Thesis

Submitted to the Department of Electrical and Electronic Engineering

and the Graduate School of Yonsei University

in partial fulfillment of the

requirements for the degree of

Master of Science

Jae-Young Kim

January 2006

This certifies that the master's thesis of Jae-Young Kim is approved.

_____

Thesis Supervisor: Woo-Young Choi

_____

Sangkook Han

_____

Hideki Kamitsuna

The Graduate School

Yonsei University

January 2006

Contents

Figure Index

Table Index

Abstract

Equivalent circuit modeling of InP/InGaAs Heterojunction Phototransistor for application of Radio-on-fiber systems

By

Jae-Young Kim

Department of Electrical and Electronic Engineering

The Graduate School

Yonsei University

In this these, equivalent circuit models of InP/InGaAs heterojunction phototransistors (HPTs) were developed focusing on the photo-detection characteristics for radio-on-fiber system applications.

The HPT DC model was developed based on the conventional Gummel-Poon equivalent circuit model. From the measured Gummel-plot, junction diodes and forward current gain were modeled. Then, the parasitic resistance values were extracted by using the open-collector and open-emitter method. The developed DC model closely describes electrical DC characteristics of HPT under dark and optical

illumination conditions.

Hybrid-π type AC small-signal model was developed by numerical fitting of simulated S-parameters to measured data. Extracted model parameters show dependence on electrical and optical bias conditions. For describing of frequency dependent photo-detection characteristics, the dual current source model was employed as AC photocurrent model. When the ratio of diffusion current is controlled by the base-collector junction voltage, the developed AC model exhibits high accuracy on describing AC characteristics of HPT.

The large-signal model was developed by combining DC and AC model components. Based on DC model, AC components such as variable capacitors and AC photocurrent model were supplemented. The developed large-signal model can describe not only DC and AC small-signal characteristics of HPT, but also large-signal characteristics such as optoelectronic mixing. Moreover, each element included in this model basically own physical meaning, so that the developed model can expect to support our analysis about the device operation.

Keywords: InP/InGaAs HPT, radio-on-fiber system, photo-detection, phototransistor, large-signal model, photocurrent model

Ⅰ. Introduction

There is a growing need for millimeter-wave wireless data transmission systems which can offer ultra-wide bandwidth. Millimeter-wave wireless communication systems require a large number of antenna base stations due to high transmission loss of millimeter waves in air. Radio-on-fiber (RoF) systems are an attractive solution for this problem because they can provide a network in which numerous antenna base stations are connected through fiber to one central office having centralized functions [1]. In this way, antenna base stations can be simple and cost-effective.

Among several different schemes for realizing millimeter-wave RoF systems, the remote up-conversion scheme is receiving much attention [2]. In this scheme, optical LO signals from the central office are shared among base stations and data are transmitted in the optical intermediate frequency (IF) domain. At the base station, transmitted IF signals are photo-detected and frequency up-converted to millimeter-wave band. Fig. 1.1 shows the block diagram of remote up-conversion scheme in radio-on-fiber systems. This scheme can provide immunity to dispersion-induced carrier suppression problems which can be very serious in millimeter-wave RoF systems [3]. However, in this

configuration, antenna base stations have to include many microwave components such as millimeter-wave mixers, local oscillators and amplifiers for frequency up-conversion. It makes antenna base stations complex and expensive, which can be a big problem in RoF systems because these systems require a large number of base stations. The monolithic integration of a photo-detector and other millimeter-wave components in antenna base station is a good approach for this problem [4].

InP/InGaAs Heterojunction Phototransistors (HPTs) are a very useful device for RoF systems because of their high responsivity and several functionalities such as optoelectronic mixing and injection locked oscillation [5-6]. Also, the HPTs can be monolithically integrated with HBTs using optoelectronic integrated circuit (OEIC) process because these devices have the fully compatible layer structure [7].

For design of OEIC, equivalent circuit models of HPTs that include optical illumination effects are required. The purpose of the paper is to establish a large-signal equivalent circuit model of an HPT, which include the optical illumination effect. The DC model was developed based on Gummel-Poon model and describes optical illumination effect with the DC photocurrent model. An electrical small-signal model was developed over several DC bias currents on base terminal and DC

optical illumination power. For describing optical modulation response of HPT, AC current model in [19] is extended. The AC photocurrent model includes dual current sources which separately represent drifting and diffusing photo-detection carriers in the absorption layer. With developed DC and AC small signal models, the large signal equivalent circuit model was accomplished. Developed large signal model can describe the effect of electrical bias and optical illumination power on AC characteristics of HPTs. Moreover, the characteristics of HPT optoelectronic mixer can be simulated with this model.

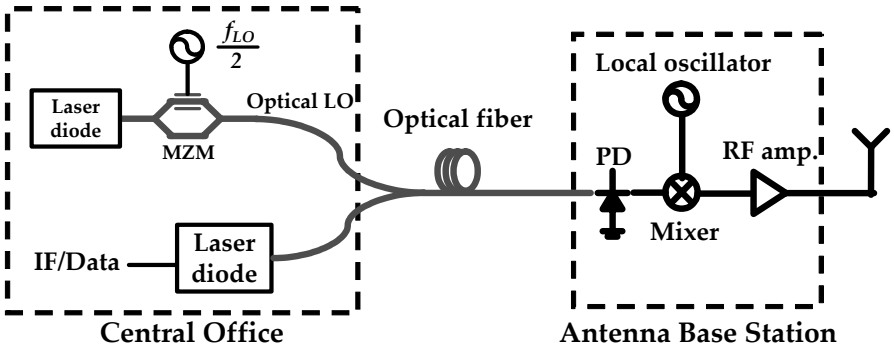

Figure 1.1 Block diagram of remote up-conversion scheme in radio-on-fiber systems

Ⅱ. Background

A. InP-based heterojunction phototransistor

The Heterojunction Photo-Transistor (HPT) is Heterojunction Bipolar Transistor (HBT) which have optical window on top of emitter for optical illumination. The InP-based HPTs are fabricated with the hetero-structure epitaxial layers grown on a semi-insulating InP substrate by using molecular beam epitaxy (MBE) or metal-organic chemical vapor deposition (MOCVD) [8]. As shown in Fig. 2.1 (a), epitaxial layer of typical single-heterojunction phototransistor is composed of n-type doped $In_{0.53}Ga_{0.47}As$ collector, p^+-doped $In_{0.53}Ga_{0.47}As$ base and n-type doped InP emitter. When the emitter-base junction is forward-biased, carriers are injected from the n-type emitter to the p^+-doped base region. These injected electrons are swept across the base region by the drift-and-diffusion process, and mostly collected by the reverse-biased collector-base junction [9]. Fig. 2.1 (b) shows energy band diagram where the emitter-base junction is forward biased and collector-base junction is reverse-biased. When optical signal is injected into the HPT, photons are mostly absorbed in the depletion region of base-collector junction and generate electron-hole pair. Then,

photo-generated electrons and holes are drifted to collector and base regions. While drifted electrons are swept in collector region, holes are accumulated in base region and lower the potential barrier of emitter-base junction resulting in increasing carrier injection from emitter to base region. As a result, photocurrent which is generated by optical illumination, flow from collector to base and induces large amount of emitter current with gain mechanism of bipolar transistors.

The advantages of HPT are high current gain and excellent microwave characteristics due to the hetero-structure of emitter-base junction. In HPT or HBT, the maximum DC current gain is expressed as [9]

$$\beta_{\max} \cong \frac{D_{n,B} N_E w_E^{'}}{D_{p,B} N_B w_B^{'}} \exp(\frac{\Delta E_g}{kT}), \quad if \ \alpha \cong \gamma_E \tag{2-1}$$

where

$D_{n,B}$ minority carrier diffusion coefficient in base

$D_{p,E}$ minority carrier diffusion coefficient in emitter

N_E doping concentration in emitter

N_B doping concentration in base

$w_E^{'}$ width of emitter depletion region

$w_B^{'}$ width of base depletion region

ΔE_g difference of bandgap energy in base and emitter

α absorption coefficient

γ_E emitter efficiency.

As one use larger bandgap material (InP) in emitter layer than that of base layer (InGaAs), a very large current gain can be obtained, even if the base doping concentration (N_B) is significantly larger than emitter doping concentration (N_E). The heavy doping in base region reduces the base resistance and allows thin base width without base punch-through. Because low base resistance and base width which are critical in reducing RC time constant of device and base transit time respectively, operation speed of transistor is improved by heavy doping in base region while maintaining the large current gain. Also, low emitter doping concentration reduces the base-emitter capacitance resulting in high speed operation [10].

As materials for emitter-base hetero-structure, InP/$In_{0.53}Ga_{0.47}As$ pair has most attractive properties, particularly for application of radio-on-fiber system. Conventional InP-based HPTs achieve higher frequency operation than GaAs or SiGe-based HPTs. The high speed operation of InP-based HPT is an important advantage for application of RoF system, because millimeter-wave band signals should be generated and

processed in this system. Recently reported InP-based HPTs have current gain cutoff frequency (f_T) and maximum oscillation frequency (f_{max}) exceeding 300GHz [10]. Moreover, InP/ $In_{0.53}Ga_{0.47}As$ HPT is suitable for detecting 1.55 ㎛ optical signal. Since the bandgap energy (0.74 eV) of $In_{0.53}Ga_{0.47}As$ material is smaller than that of photon (0.8 eV) at wavelength of 1.55 ㎛, optical signal can be absorbed in depletion region of base-collector junction. The transparency of InP emitter layer for 1.55 ㎛ photon make it easy to illuminate optical signals on base-collector junction [8].

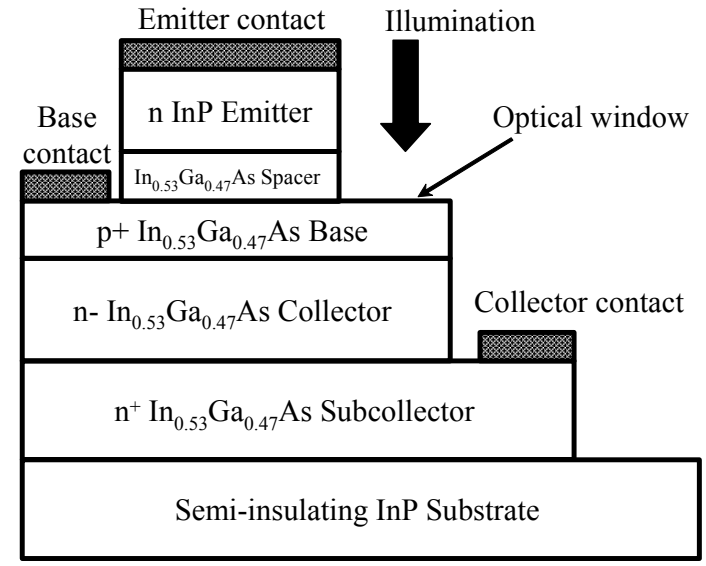

(a)

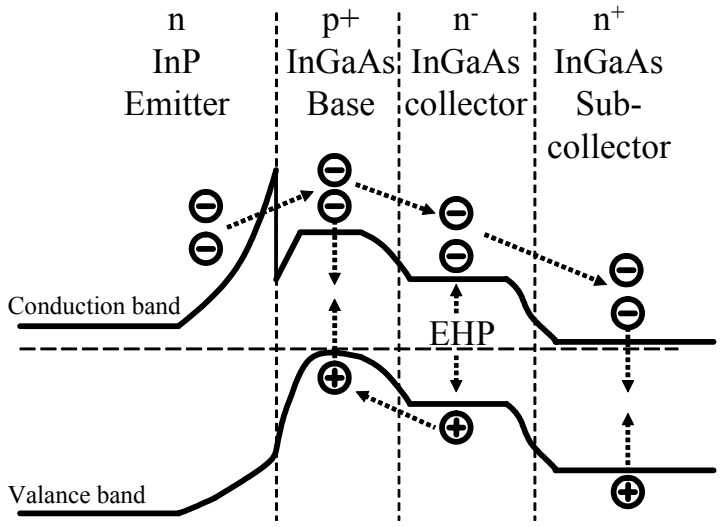

(b)

Figure 2.1 Conventional InP-based HPT (a) Epitaxial layer structure (b) Energy band diagram.

B. InP/InGaAs heterojunction phototransistor used in this Thesis

The device used in this thesis is InP/InGaAs single-heterojunction N-p-n HPT[1] with 70 nm thick InP undoped emitter. The base layer is 50nm thick $In_{0.53}Ga_{0.47}As$ with carbon doping of 3.7×10^{19} cm^{-3}. The collector layer is 300nm thick $In_{0.53}Ga_{0.47}As$ [11]. Epitaxial layer structure is shown in Fig. 2.2. Optical window with 5 μm diameter is located on the top of emitter layer. With top-illumination, the HPT exhibits responsivity of 0.2A/W.

At forward active bias condition, DC current gain of this HPT is about 50. With collector bias voltage of 1.0V and current of 17mA, the current gain cutoff frequency (f_T) and maximum oscillation frequency (f_{max}) are 141GHz and 84GHz, respectively. At the same bias point, optical gain cutoff frequency is 68GHz. The optical gain cutoff frequency is defined as optical modulation frequency where the frequency response in phototransistor mode intersects the low-frequency response in photodiode mode.

[1] The undoped emitter InP/InGaAs HPT used in this thesis is provided by Photonics Laboratories in NTT, Japan.

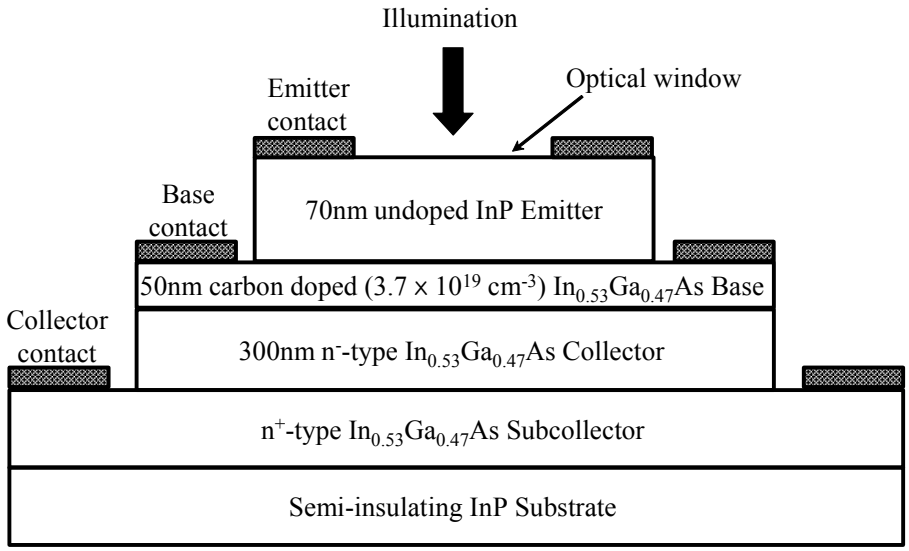

Figure 2.2 Epitaxial layer structure of the undoped emitter InP/InGaAs HPT used in this thesis.

Ⅲ. DC modeling of InP/InGaAs HPT

A. Electrical characteristics and modeling

DC characteristics of InP/InGaAs HPT were measured with semiconductor parameter analyzer (HP4145B) to establish DC equivalent circuit model. Fig. 3.1 shows the schematic diagram of developed DC model which is based on Gummel-Poon bipolar model [12]. The base current is represented by two sets of parallel diodes which correspond to base-emitter junction and base-collector junction separately. In each set, one diode describes the simple voltage-current relationship of p-n junction, while the other one represents the recombination current in the space-charge region of each junction at low bias voltage. The ideality factors and reverse saturation currents of diode models corresponding to base-emitter junction were extracted with forward Gummel-plot as shown in Fig. 3.2 (a). Similarly, the parameters corresponding to base-collector junction were obtained with reverse Gummel-plot shown in Fig. 3.3.

In contrast to homo-junction bipolar transistors, forward current gain (β_f) of heterojunction bipolar transistor is not constant at forward bias region. Some previous research has attempted modeling of this

property with collector current dependent current gain model [13] or high recombination current model in space charge region [12]. However, these approaches don't show so good accuracy on describing the forward current gain of used HPT. Our DC model describes the forward current gain as a function of base-emitter voltage shown below.

$$\beta_f = \frac{58.3}{1 + 3.275 \cdot 10^3 \cdot e^{-11.034 \cdot V_{BE}}} \tag{3-1}$$

This numerical function was obtained from forward current gain graph versus base-emitter voltage as shown in Fig. 3.2 (b), where the graph is simply extracted from forward Gummel-plot. Reverse current gain (β_r) was estimated as 0.022 with reverse Gummel-plot.

The parasitic base and emitter resistances (R_B and R_E) were extracted by the open-collector method [14] which is shown in Fig. 3.4 (a). When collector port is open, the voltage across base-collector junction and collector resistance are negligible. So, measured collector voltage (V_C) indicates the voltage of intrinsic base region. Then, R_B and R_E can be estimated by the ratio of base and collector voltages (V_B and V_C) variation over change of supplied base current (I_B). The voltage across base-emitter diode is assumed as not sensitive for current variation in this method. But, in this research, voltage drop across base-emitter and

base-collector junction diodes are considered for more accurate estimation of parasitic resistance values. V_B and V_C over I_B are simulated using the equivalent circuit model that contains previously obtained diode model parameters as shown in Fig. 3.4 (b). The values of R_B and R_E are obtained by fitting of simulation results with measured V_B and V_C as shown in Fig. 3.5 (a). For estimation of collector resistance (R_C), a similar process was done. In emitter-open condition, V_B and V_E were measured and simulated over change of supplied I_B as shown in Fig. 3.5 (b).

DC model parameters obtained by the explained modeling procedure are shown in Table 3. 1. With the developed DC model, I_C-V_C characteristics for several base current bias conditions were simulated and compared with measured data as shown in Fig. 3.6. Simulation results are well-matched with measured data.

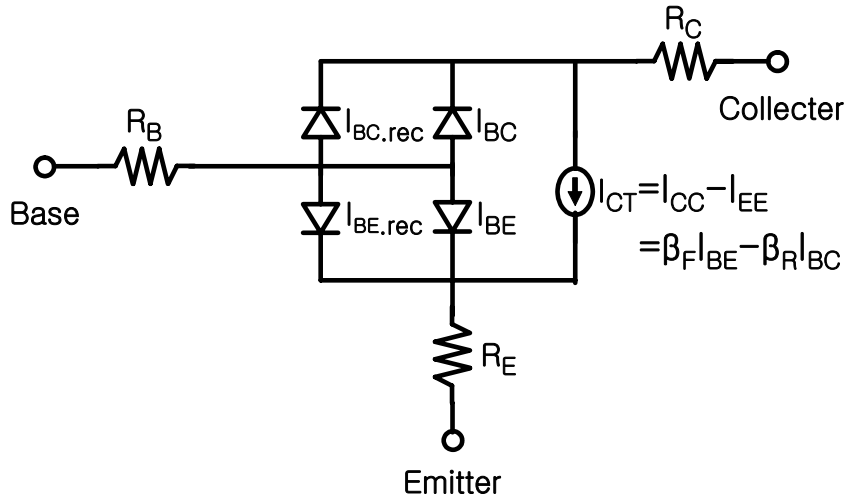

Figure 3.1 Developed DC model of InP/InGaAs HPT

parameter		value	parameter		value
I_{BE}	n	1.53	$I_{BE.rec}$	n	8
	Is	8.16×10^{-14} A		Is	4×10^{-10} A
I_{BC}	n	1.032	$I_{BC.rec}$	n	1.593
	Is	1.71×10^{-13} A		Is	7.47×10^{-11} A
R_B		28 Ω			
R_C		3.9 Ω			
R_E		0.5 Ω			

Table 3.1 DC model parameters (n is ideality factor, and Is is reverse saturation current of diode)

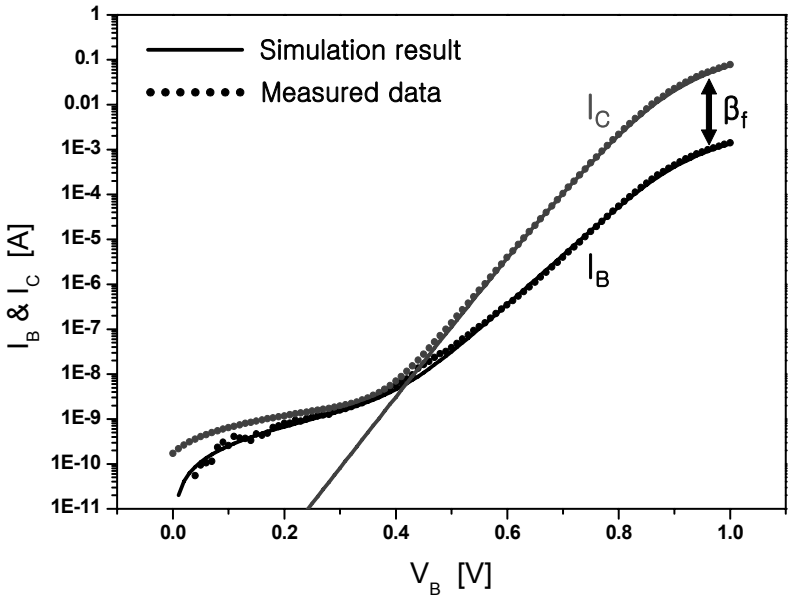

(a)

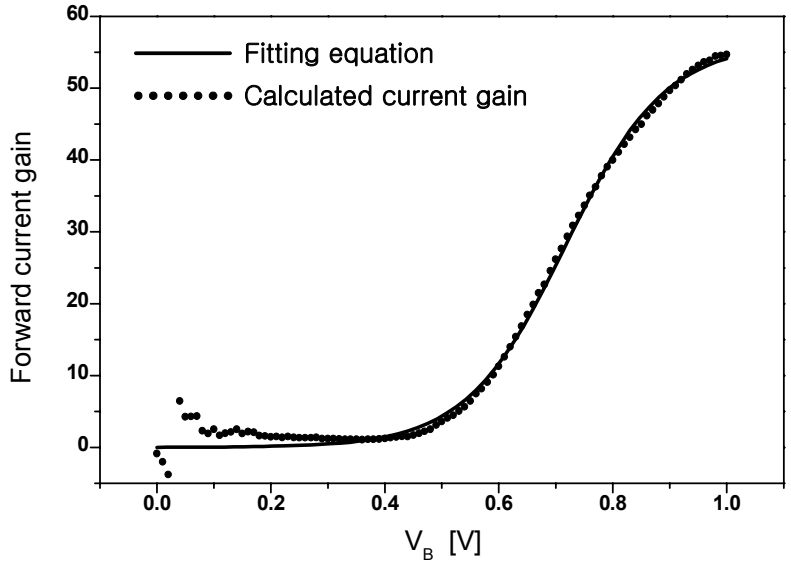

(b)

Figure 3.2 (a) Forward gummel plot (I_B and I_C versus V_{BE} where V_B=V_C) (b) Fitting result of forward current gain versus V_{BE} (calculated from (a)) with a numerical function

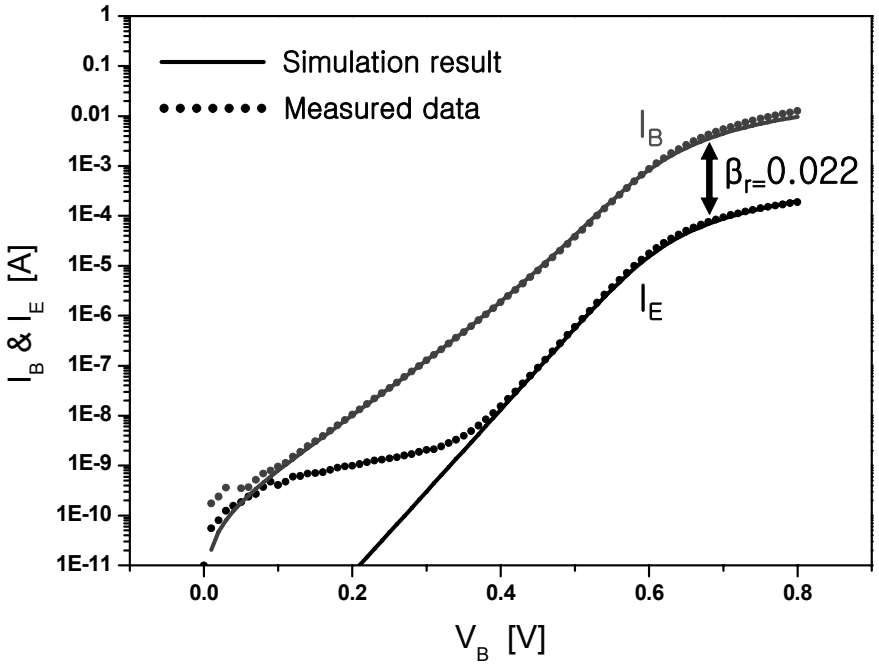

Figure 3.3 Reverse gummel plot (I_B and I_E versus V_{BE} where V_B=V_E)

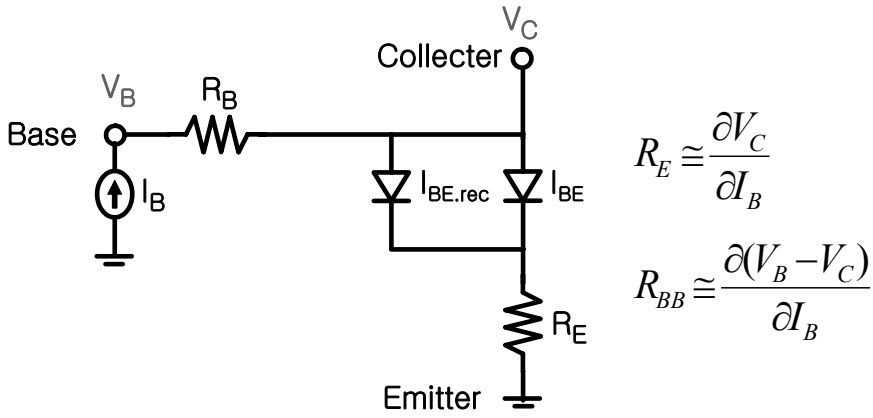

(a)

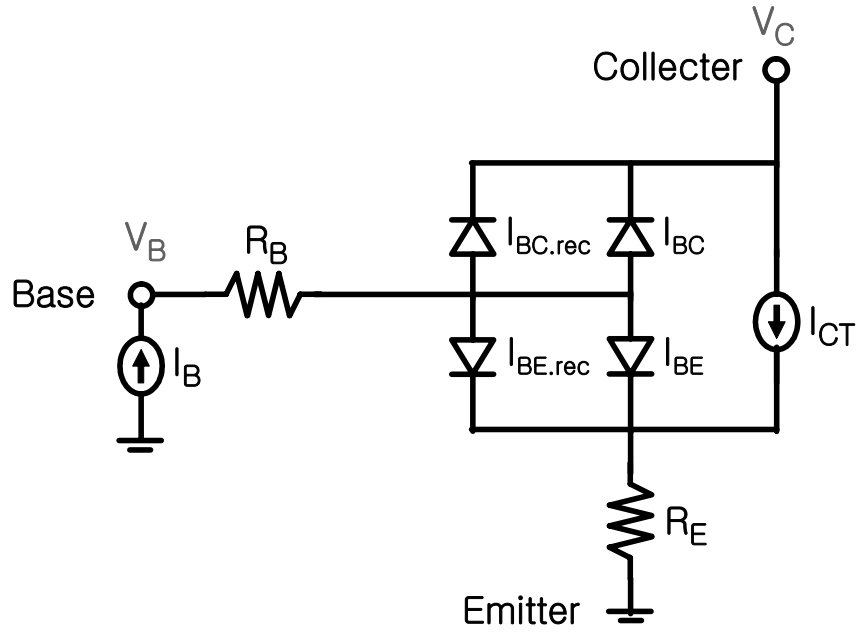

(b)

Figure 3.4 Open-collector method (a) schematic for rough estimation (b) schematic diagram for more accurate simulation and fitting

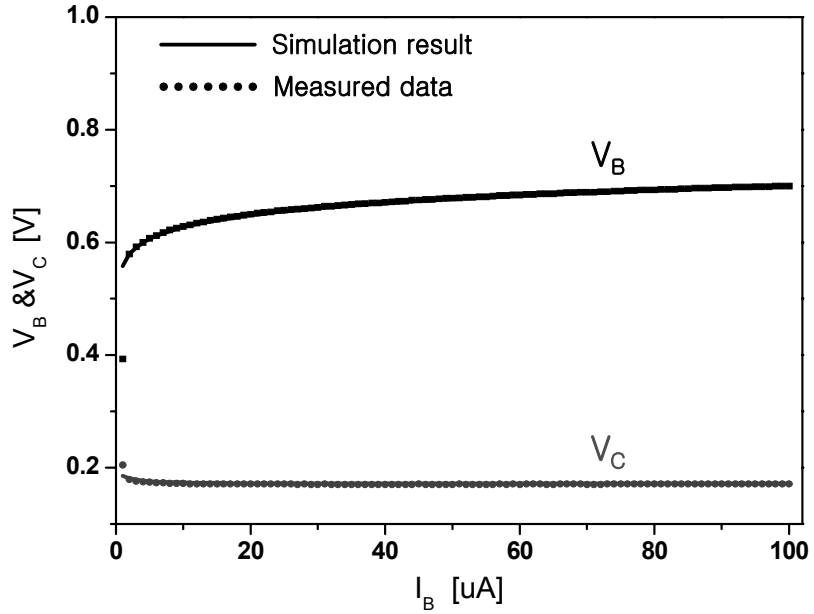

(a)

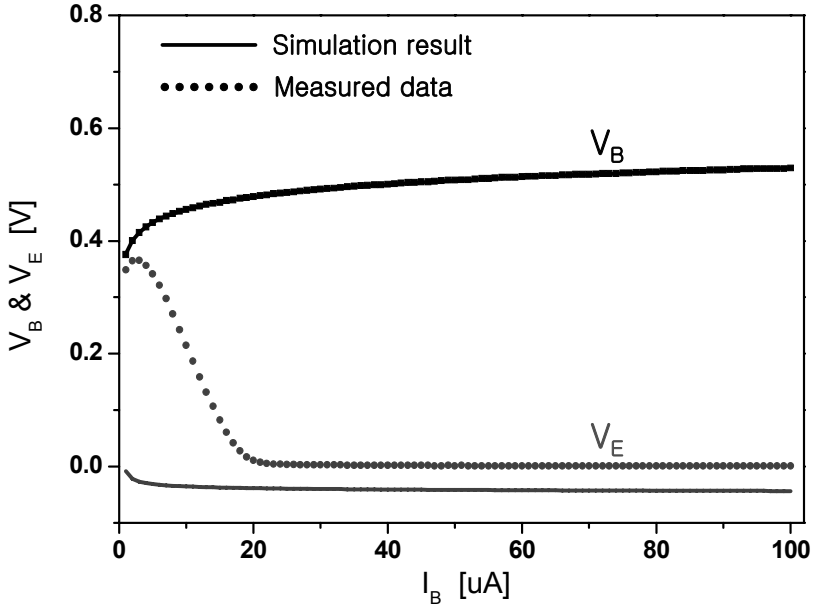

(b)

Figure 3.5 Comparison between measured and simulated (a) V_B and V_C versus supplied I_B where I_C=0 (b)) V_B and V_E versus supplied I_B where I_E=0

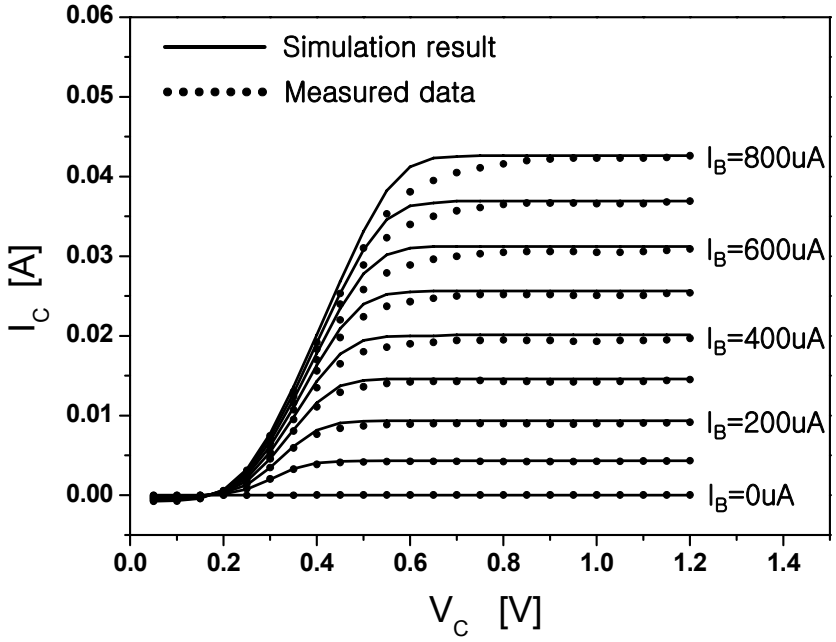

Figure 3.6 Comparison between measured V_C-I_C characteristic on constant base current (0μA, 100μA…… and 800μA) and simulation result using developed DC model

B. Optical characteristics and modeling

DC characteristics of InP/InGaAs HPT are measured with semiconductor parameter analyzer (HP4145B) under optical illumination condition. Collector current versus collector voltage in optical illumination condition is measured and compared with that in dark condition. Fig. 3.7 (a) compares I_C-V_C characteristics when input optical power is 0dBm with that in dark condition. Optical illumination of moderate power gives similar effect on I_C-V_C characteristic as electrically induced base current. However, at high power optical illumination, the HPT exhibits abnormal characteristics. In this region, optically generated photocurrents have higher current gain than electrically injected base currents as shown in Fig. 3.7 (b).

As previously explained, DC optical illumination generates DC photocurrents which flow from collector region to base region and lower the potential barrier of emitter-base junction as like electrically injected DC base current. So, optical illumination on HPTs was modeled with a current source across intrinsic base-collector junction which describes photocurrent of base-collector depletion region [15] as shown in Fig. 3.8 (a). Optical illumination power of 0dBm is modeled by photocurrent of 200μA, which agrees with photocurrents calculated

from HPT responsivity of 0.2A/W. Fig. 3.8 (b) compares measured I_C-V_C characteristic when input optical power is 0dBm with the simulation results. The simulation results are well-matched with measured data.

The abnormal characteristic of HPT at high power optical illumination shown in Fig. 3.7 (b) is not analyzed yet. More research needs to be done in order to understand this phenomenon.

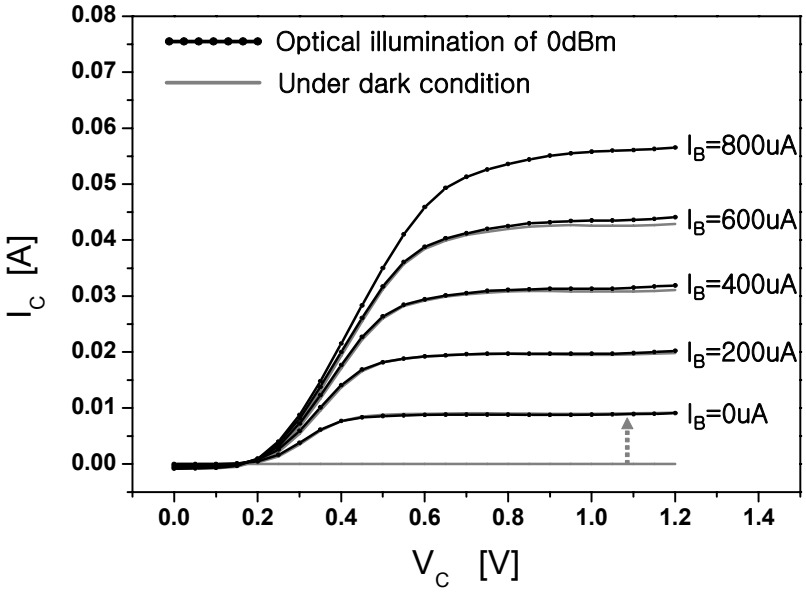

(a)

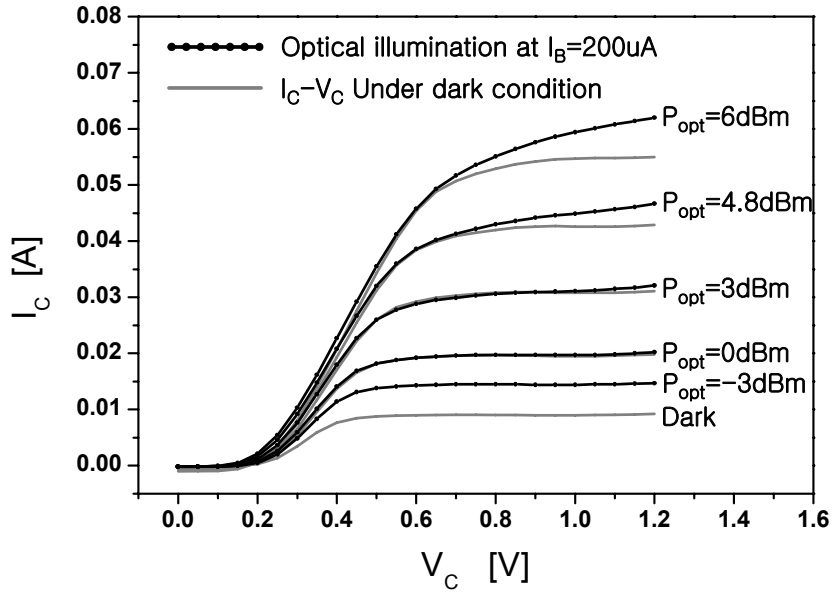

(b)

Figure 3.7 Measured I_C-V_C characteristic at (a) optical power is 0dBm and base current is 0㎂, 200㎂…… 800㎂ (b) base current is 200㎂ and optical power is -3, 0, 3, 4.8 and 6dBm

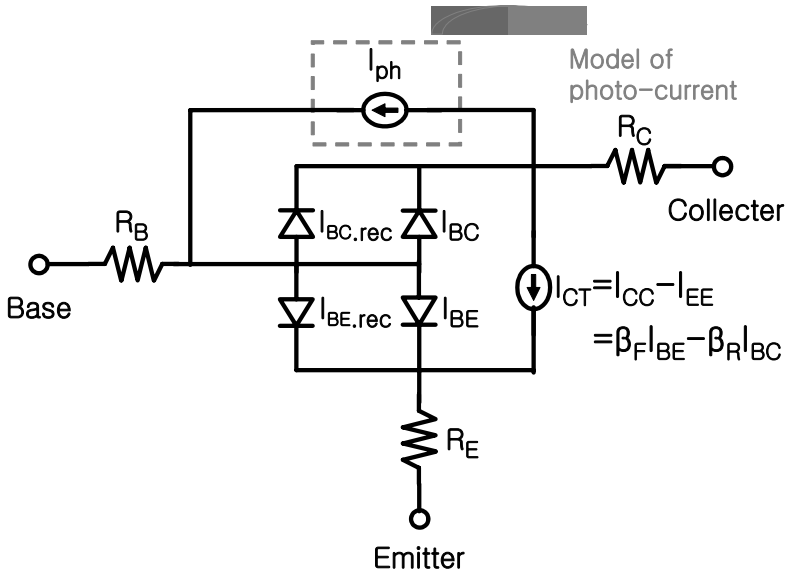

(a)

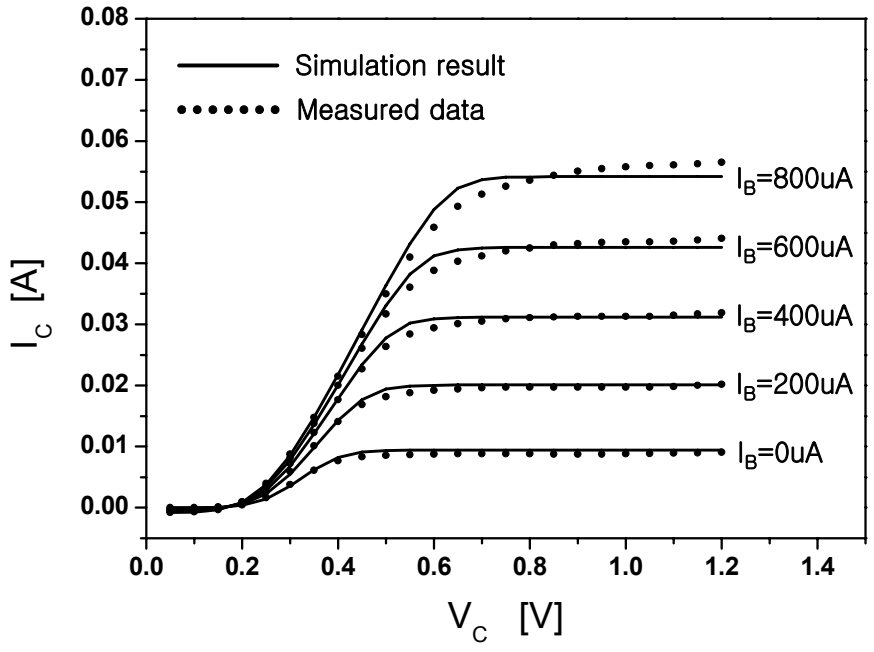

(b)

Figure 3.8 (a) Complete DC model of InP/InGaAs HPT including photocurrent (b) Comparison between measured V_C-I_C characteristic in 0dBm optical illumination condition and simulation result using (a)

Ⅳ. AC small-signal modeling

A. Electrical AC characteristics and modeling

AC small-signal model of InP/InGaAs was developed based on conventional hybrid-π model as shown in Fig. 4.1. In this model, capacitances (C_{BC_ext}, C_{BC_int}, C_C) over base-collector junction are separately represented to describe high frequency operation of InP-based HPTs. The parallel RC combination (C_{BP} // R_{BP}) of base region represents distributed base contact impedance [16].

The S-parameters were measured with network analyzer (HP E8364B) from 45MHz to 50GHz for extraction of model parameters. The parasitic components of HPT on-wafer pad structure were eliminated with the de-embedding technique based on open and short test structures [16]. After that, small-signal model parameters were extracted by numerical fitting of simulated S-parameter to measured data. Fig. 4.2 shows comparison of measured and simulated S-parameters, where I_B and V_C are 200㎂ and 1V, separately.

The parameter extraction was done for I_B bias point from 0㎂ to 800㎂ with 200㎂ step where V_C is 1V in dark condition, and the dependence of small-signal parameters on base current was observed

and summarized in Table. 4.1. Capacitance components of base-emitter and base-collector junction increase exponentially with base current. Theoretically, increasing current causes exponential increment of diffusion capacitance in the junction [17]. So, C_{BE} has exponential dependency on the supplied base current. On the other hand, increasing of base current increases the voltage of intrinsic base region resulting in decrease of base-collector junction voltage. So, base current dependences of base-collector capacitances can be analyzed as the increasing of junction capacitances. Fig. 4.3 shows comparison of measured and simulated S-parameters on bias condition of I_B=800㎂ and V_C=1V.

Similar process was done for changing of input optical power (-3, 0, 3 and 4.8dBm) under the bias condition of I_B=200㎂ and V_C=1V. The dependences of small-signal model parameters on input optical power are shown in Table 4.2. In DC characteristics of HPTs, the optical illumination of 0dBm can be modeled by photocurrent of 200㎂ and the effects of photocurrent are similar with that of electrical base current. Also in AC characteristics, the measured S-parameters of same collector current and voltage (I_B=400㎂, V_C=1V and dark condition ↔ I_B=200㎂, V_C=1V and optical illumination power of 0dBm) were almost same. So, dependence of small-signal model parameters on

input optical power is similar with that on electrical base current bias.

The effect of collector voltage on small-signal model parameters was also investigated. Collector voltage was changed from 1V to 1.5V where I_B is 400μA and optical power is 0dBm. As summarized in Table 4.2, the collector voltage mainly affects capacitance components of base-collector junction, because increasing collector voltage makes widening of base-collector depletion region. Fig. 4.4 shows comparison of measured and simulated S-parameters where I_B=400μA, V_C=1.5V and optical power is 0dBm.

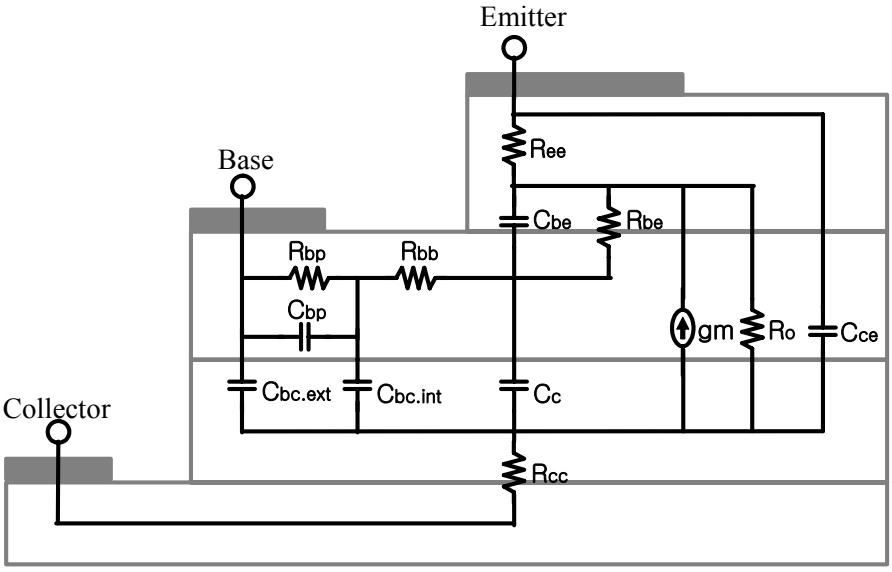

(a)

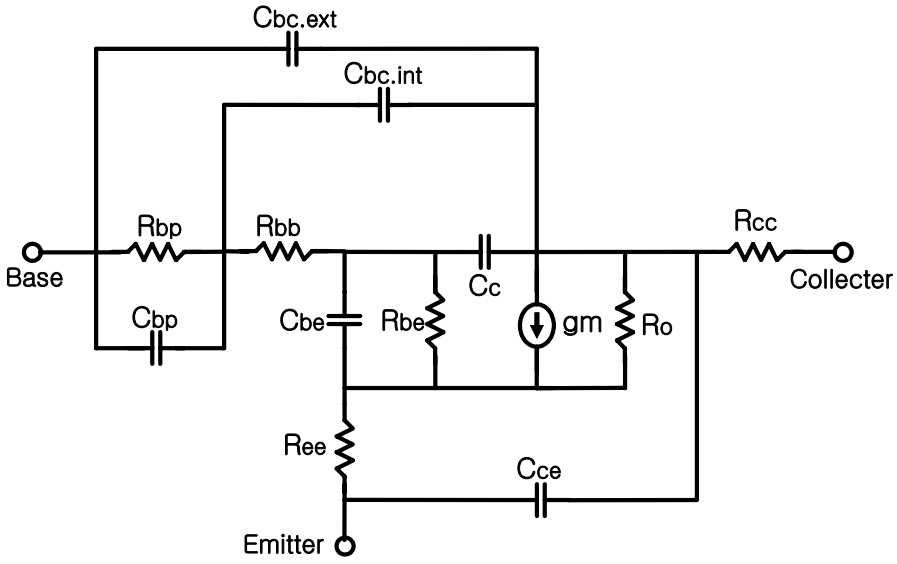

(b)

Figure 4.1 (a) equivalent circuit elements in cross section of InP/InGaAs HPT (b) schematic diagram of small-signal equivalent circuit model of HPT

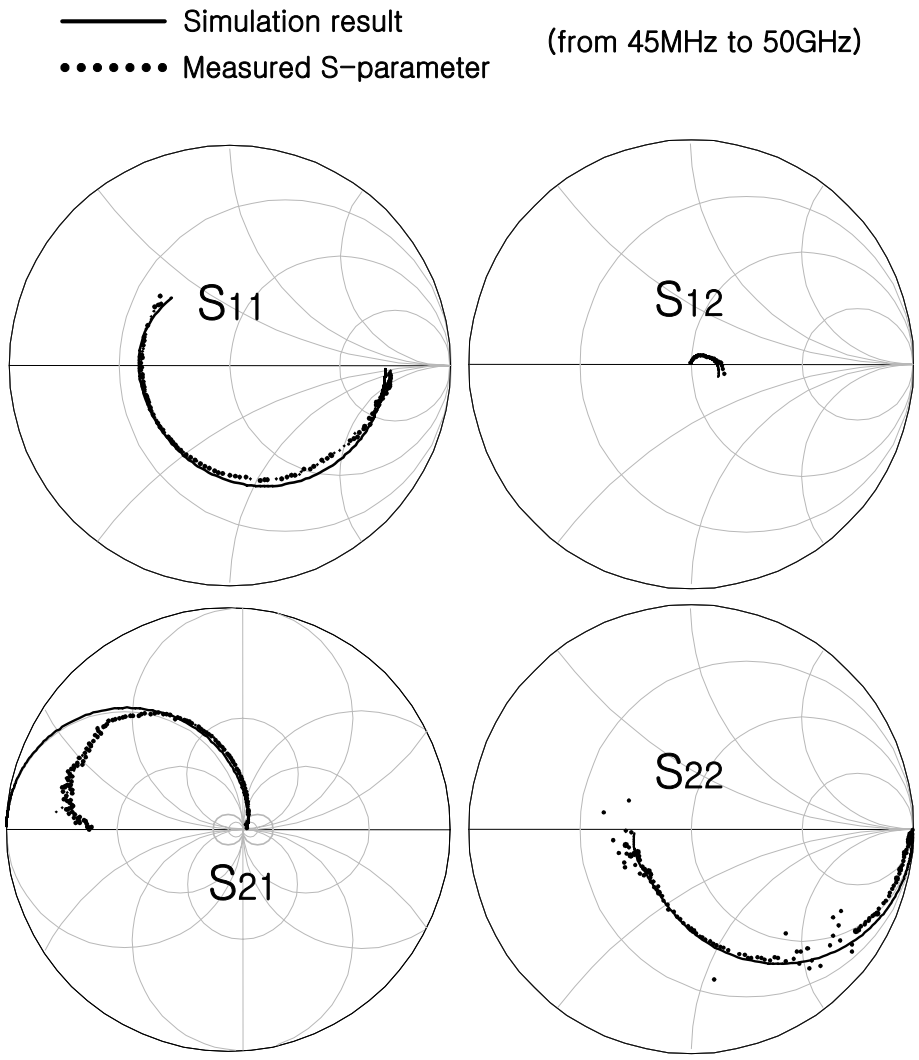

Figure 4.2 Comparison of measured and simulated S-parameters, where I_B and V_C are 200μA and 1V in dark condition

I_B	0uA	200uA	400uA	600uA	800uA
R_{CC} [Ω]	3.7				
R_{EE} [Ω]	0.48				
R_{BB} [Ω]	12.5				
R_{BP} [Ω]	16.4				
C_{BP} [fF]	250				
$C_{BC.EXT}$ [fF]	15	16.7	18.6	25.9	28.6
$C_{BC.INT}$ [fF]	9				
C_C [fF]	12.3	18.6	18.5	24	30
C_{CE} [fF]	25				
C_{BE} [fF]	74.3	304	430	734	1096
R_{BE} [Ω]	-	233	91	44	21
gm_o [mS]	-	217	435	697	1100
R_O [Ω]	∞				
τ [pS]	0.2				

Table 4.1 Dependences of small-signal model parameters on base current bias. The parameters were extracted on I_B bias point from 0μA to 800μA with 200μA step, where V_C is 1V in dark condition.

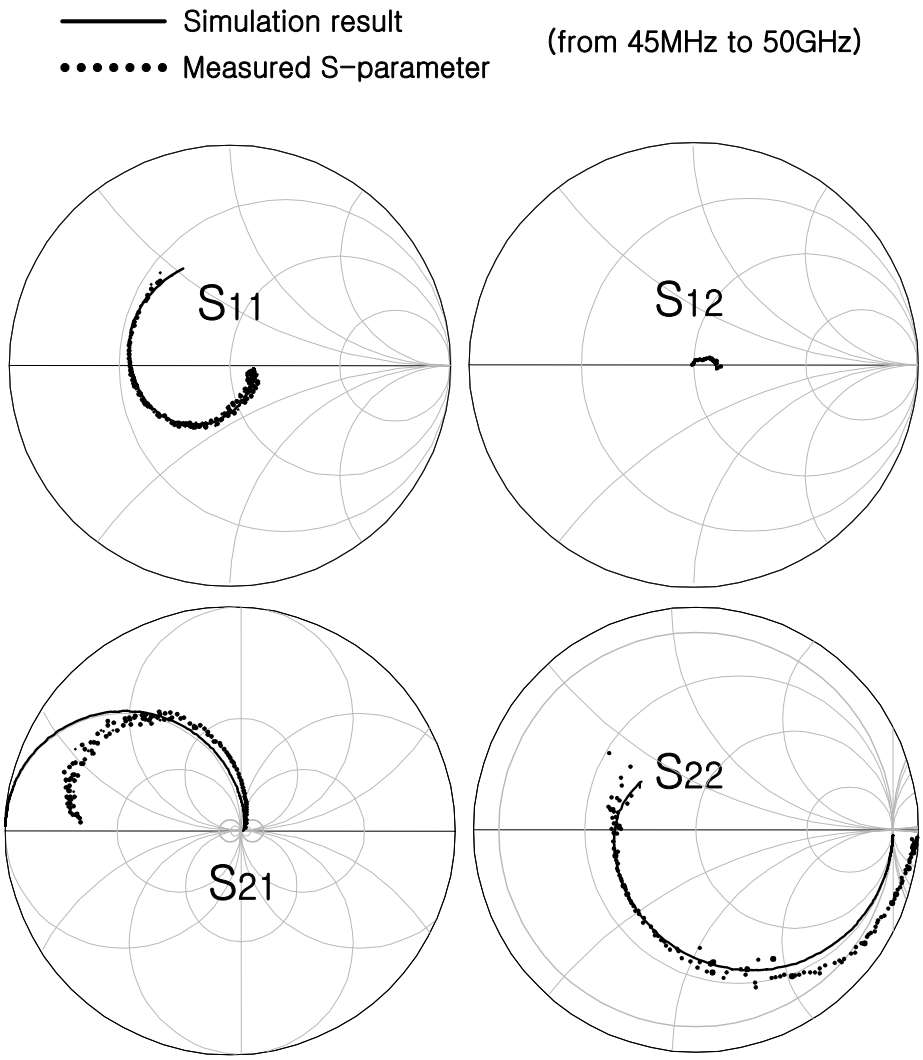

Figure 4.3 Comparison of measured and simulated S-parameters, where I_B and V_C are 800μA and 1V in dark condition

P_{opt}	Dark	-3dBm	0dBm	3dBm	4.8dBm
R_{CC} [Ω]	3.7				
R_{EE} [Ω]	0.48				
R_{BB} [Ω]	12.5				
R_{BP} [Ω]	16.4				
C_{BP} [fF]	250				
$C_{BC.EXT}$ [fF]	16.7	18.2	20.2	25.6	31.9
$C_{BC.INT}$ [fF]	9				
C_C [fF]	18.6	19.7	20.5	26	38.3
C_{CE} [fF]	25				
C_{BE} [fF]	304	367	451	667	917
R_{BE} [Ω]	233	146	99	53	31
gm_o [mS]	217	298	435	619	850
R_O [Ω]	∞				
τ [pS]	0.2				

Table 4.2 Dependences of small-signal model parameters on input optical power. The parameters were extracted on input optical power of -3, 0, 3 and 4.8 dBm, where I_B and V_C are 200μA and 1V.

V_C	1	1.2	1.4	1.5
R_{CC} [Ω]	3.7			
R_{EE} [Ω]	0.48			
R_{BB} [Ω]	12.5			
R_{BP} [Ω]	16.4			
C_{BP} [fF]	250			
$C_{BC.EXT}$ [fF]	25.9	17	16.2	15.6
$C_{BC.INT}$ [fF]	9			
C_C [fF]	24	15.8	13.8	12.4
C_{CE} [fF]	25			
C_{BE} [fF]	734			
R_{BE} [Ω]	44.1	54.8	63	67
gm_o [mS]	697			
R_O [Ω]	∞	900	484	376
τ [pS]	0.2			

Table 4.3 Dependences of small-signal model parameters on collector voltage. The parameters were extracted on collector voltage of 1, 1.2, 1.4 and 1.5V, where I_B is 400㎂ and input optical power is 0dBm.

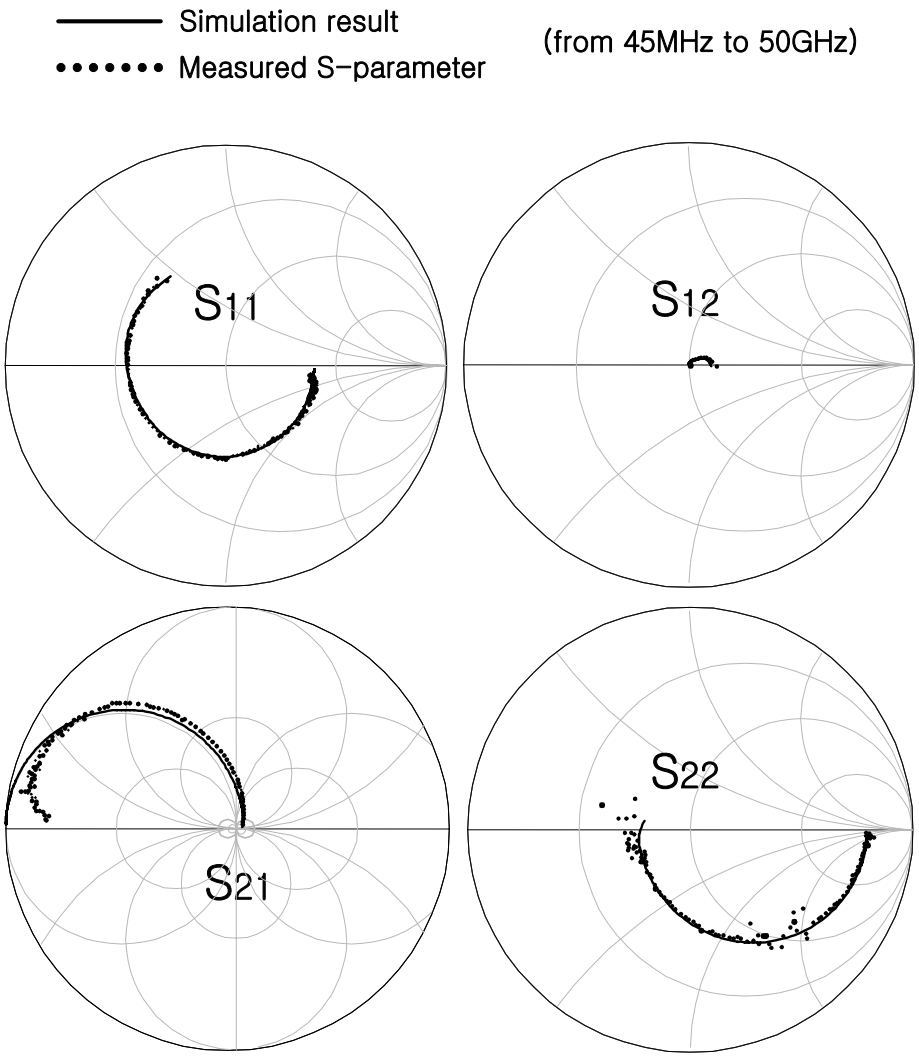

Figure 4.4 Comparison of measured and simulated S-parameters, where I_B and V_C are 400μA and 1.5V and optical power is 0dBm.

B. Optical AC characteristics and modeling

For high-speed phototransistor and optoelectronic mixer applications, the photonic bandwidth and photo-detection gain are important parameters. We investigated and analyzed frequency dependent photo-detection characteristics of InP/InGaAs HPTs by measuring optical modulation response over input power of optical signal. Then, optical AC characteristic of HPT was modeled with an AC photocurrent model based on the analysis about photo-detection mechanism.

(B.1) Optical AC characteristics of InP/InGaAs HPT

As shown in Fig. 4.5 (a), optical modulation response was measured with network analyzer from 45MHz to 20GHz. DFB laser diode (DFB LD) was directly modulated by RF signal from network analyzer, and generated optical signal was injected into the HPT through lensed fiber. RF signal detected on collector terminal was measured on the other port of network analyzer. Calibration of laser diode and optical link was performed with a high speed photodiode that can operate up to 20GHz. Fig. 4.5 (b) shows measured optical modulation response where I_B and V_C is 200μA and 1V and input optical power is 0dBm.

The experimental results show that the photonic bandwidth of HPT is inversely proportional to input optical power and base current in Fig. 4.6. This phenomenon is analyzed by simulation of optical modulation response using developed small-signal models. As shown in Fig. 4.7, the incident optical signal is modeled by an AC current source over base-collector junction. The bandwidth of simulated optical modulation response is also inversely proportional to optical power and base current as shown in Fig. 4.6. The dominant parameters that cause photonic bandwidth reduction over input optical power are $C_{BE,}$ $C_{BC.EXT}$ and C_C [18]. These capacitances exponentially increase as optical power increases. The bandwidth reduction effect is also observed on high base current condition with same reason.

But, simulated photonic bandwidth is larger than the bandwidth of measured optical modulation response. This means that, in photo-absorption process, there is another phenomenon which is not included in developed small-signal model. So, AC small-signal model of HPT was supplemented with additional analysis on this anomalous phenomenon.

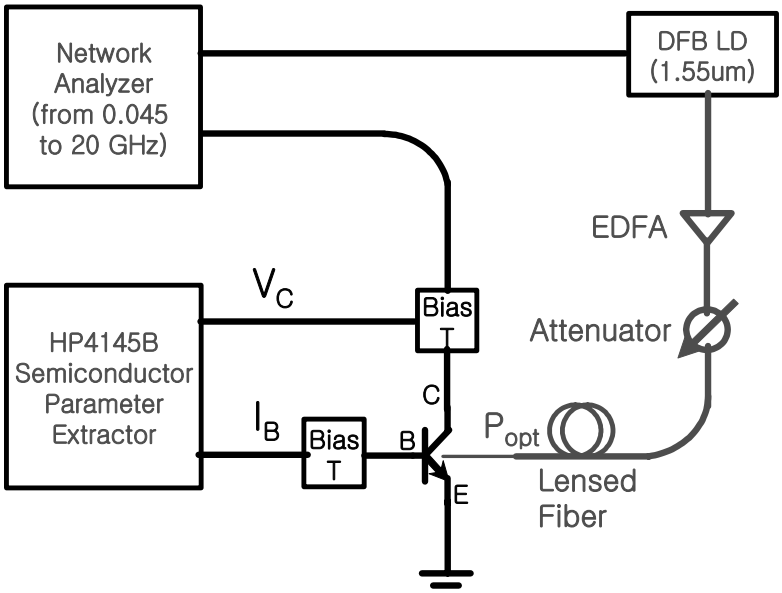

(a)

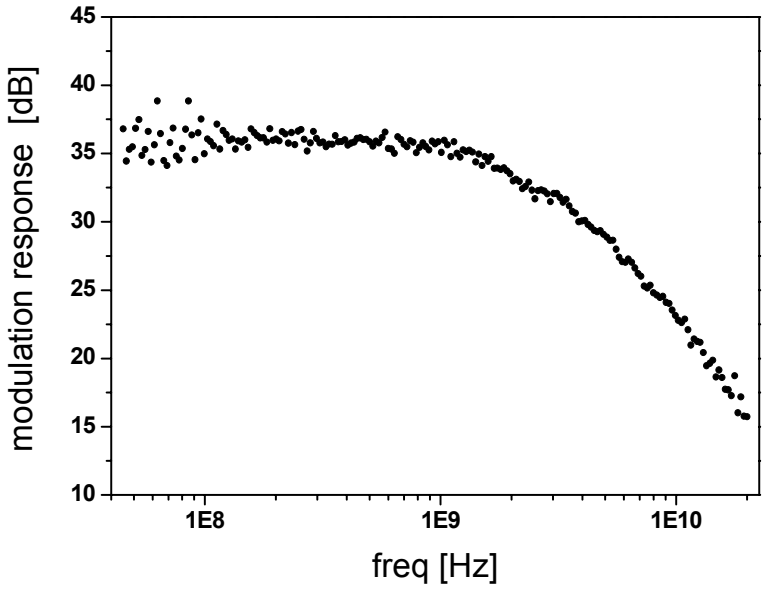

(b)

Figure 4.5 (a) Measurement setup for optical modulation response of InP/InGaAs HPT (b) Measured optical modulation response, where I_B and V_C are 200㎂ and 1V and optical power is 0dBm.

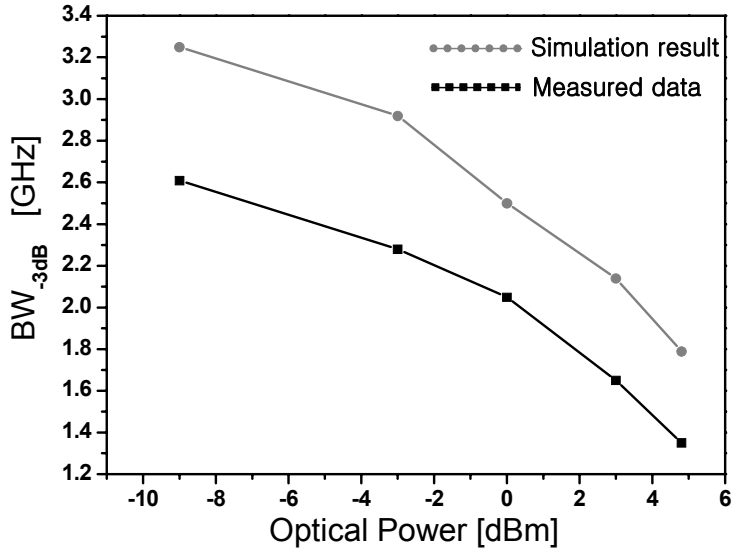

(a)

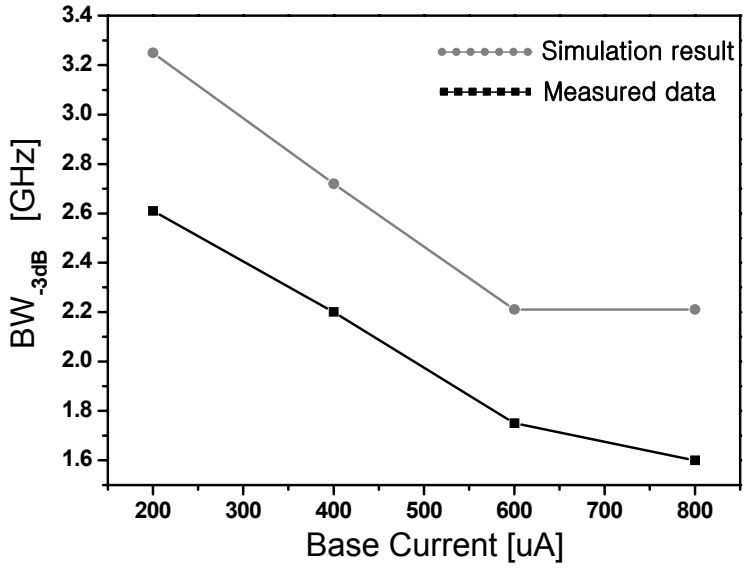

(b)

Figure 4.6 3dB bandwidth of measured and simulated optical modulation response (a) versus input optical power, where I_B and V_C are 200μA and 1V (b) versus base current, where V_C is 1V and optical power is 0dBm.

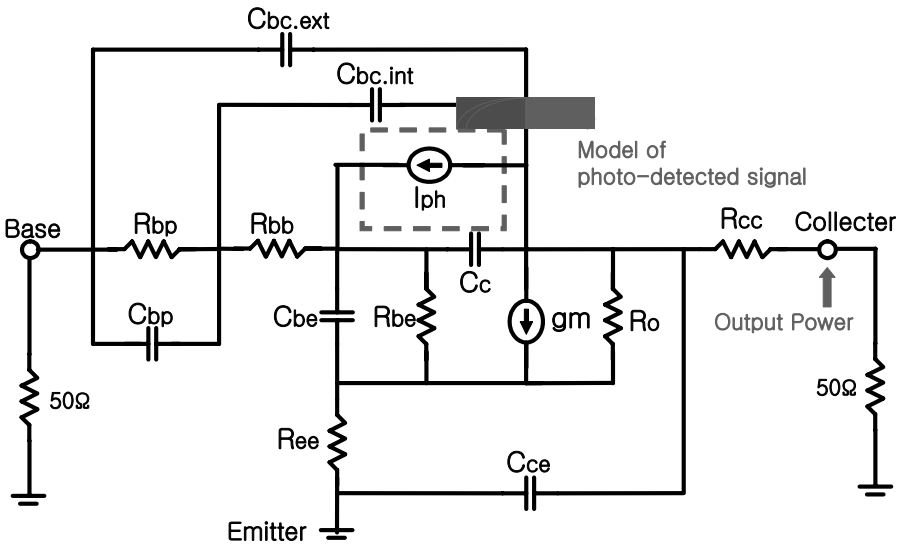

Figure 4.7 Schematic diagrams for simulation of optical modulation response. Optical input signal is modeled with single AC current source. Small-signal model parameters which were extracted from S-parameters were employed in this simulation.

(D.2) Dual current source model for photo-response

As shown in Fig. 4.8, there is some difference between measured optical modulation response and simulated response with the electrical model. In this model, photocurrent was modeled by single current source that describe only high-speed carrier absorbed in depletion region of base-collector junction. Consequently, simulated bandwidth of photo-response is limited by RC time constant of circuit model. However, in real photo-detection, a part of photons pass through the depletion region and are absorbed in neutral region of sub-collector where the electric field is very small. The low-speed holes generated in neutral region diffused into depletion region and limits high-speed operation of HPT. The coexistence of high-speed and low-speed carriers separately absorbed in depletion and neutral region was described with dual current source photo-current model [19] as shown in Fig. 4.8. By assuming the 3dB bandwidth of low-speed carrier as 1.2GHz [19], the ratio of low-speed carrier was optimized as 8% with fitting of simulated optical modulation response to measured result, where I_B and V_C are 400μA and 1.2V and input optical power is 0dBm. The measured and simulated optical modulation responses are shown in Fig. 4.9.

In previous result, the small ratio of low-speed carrier means that a major portion of input optical power was absorbed in depletion region of base-collector junction. However, if the depletion region became narrower, the ratio of photons absorbed in neutral region will increase as described in Fig 4.10 (a). When I_B and V_C are 400μA and 1V and input optical power is 0dBm, the calculated value of V_{CB} from developed DC model is -0.03V. In this low V_{CB}, which is insufficient for reverse biasing of base-collector junction, the depletion width of base-collector junction can be reduced to increase the ratio of low-speed diffusion carrier. In this bias condition, the ratio of low-speed carrier was optimized as 14% with fitting of simulation result to measured data. Fig. 4.10 (b) shows comparison of simulated optical modulation response to measured data. Fig. 4.11 (a) shows the difference between 3dB bandwidth of measured photo-response and that of simulation result. Dual current source model is more accurate than single current model, particularly in low collector voltage. The ratio of low-speed current is inversely proportional to collector voltage as shown in Fig. 4.11 (b). It is because the width of depletion region depends on applied bias over base-collector junction.

The ratio of low-speed carrier also depends on input optical power and base current. Input optical power and base current bias affects on

potential of intrinsic base region. So, the voltage across base-collector junction is changed by the amount of base current or DC photocurrent, where collector voltage is fixed. Fig. 4.12 shows fitting result of simulated photo-response on measured data using single and dual current source model, where I_B and V_C are 200μA and 1V, separately. The simulation result closely fit to measured data with dual current source model over changing of input optical power. The ratio of low-speed carrier depends on input optical power as shown in Fig. 4.13 (a). Also on base current bias, the diffusion carrier ratio has dependency as shown in Fig. 4.13 (b).

With changing collector voltage, input optical power or base current, the optical modulation response of InP/InGaAs HPT was successfully modeled with dual current source model at several DC operating points. At each bias point, the ratio of diffusion current was optimized by fitting, and the voltage across base-collector junction was extracted from developed DC model. In all of these operating points, the ratio of low-speed carrier exhibits consistent relationship with collector-base bias voltage as shown in Fig. 4.14.

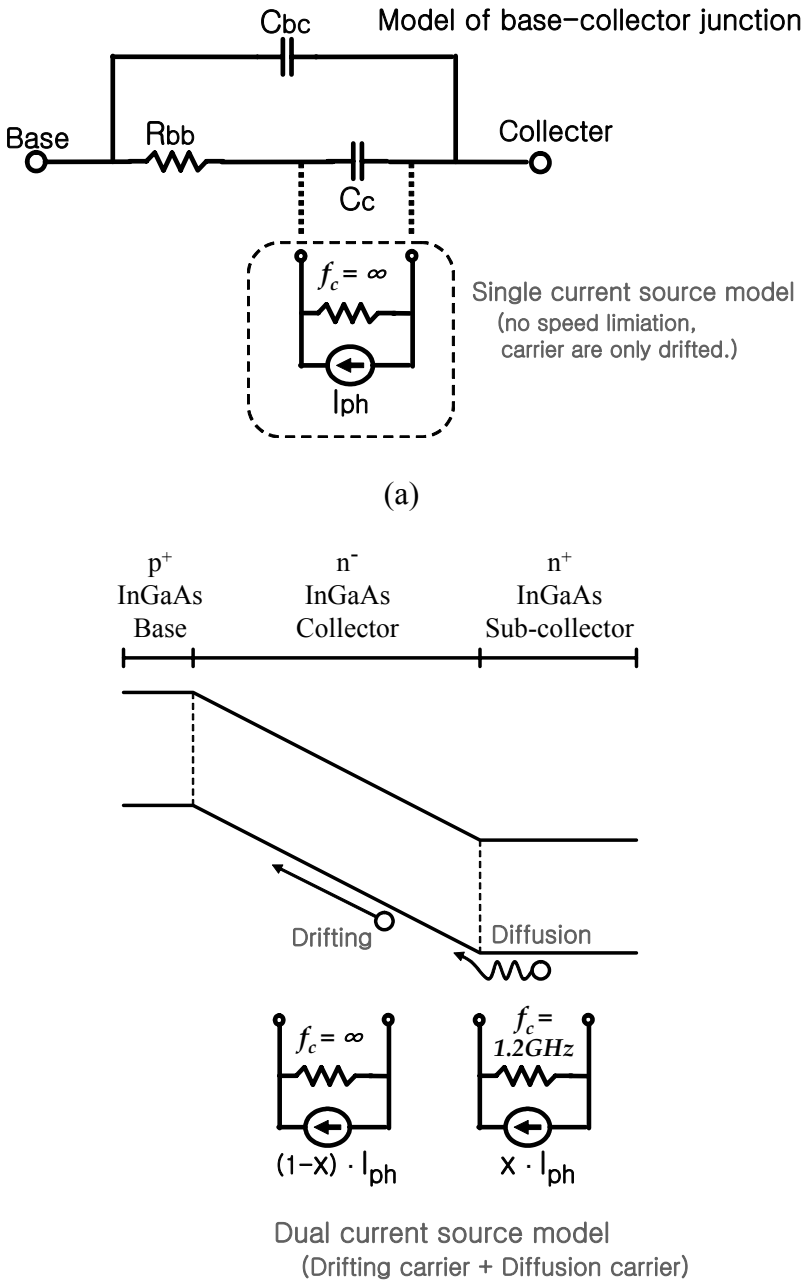

Figure 4.8 Photocurrent model (a) Conventional single current source model (b) Dual current source model

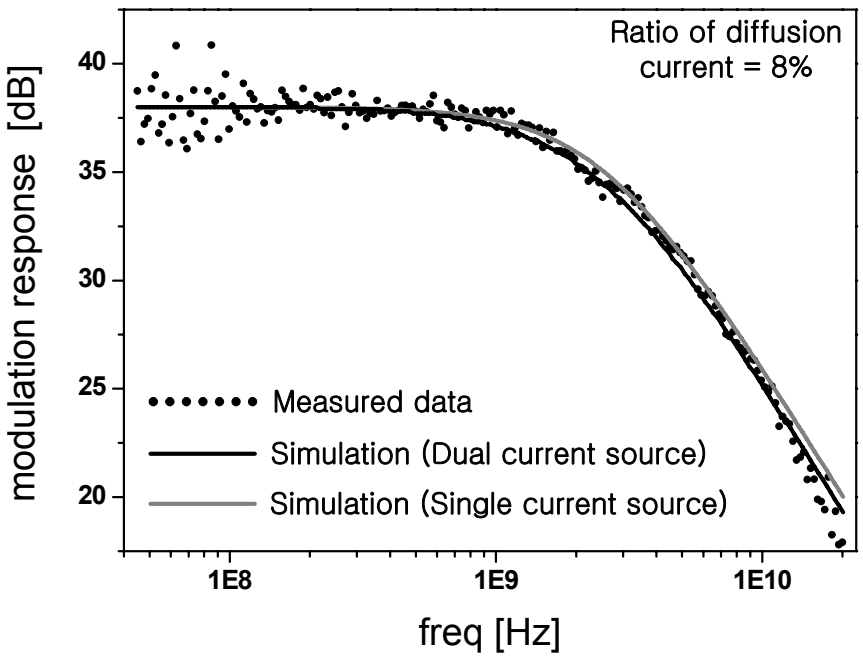

Figure 4.9 Comparison of measured and simulated optical modulation response, where I_B and V_C are 400μA and 1.2V and input optical power is 0dBm.

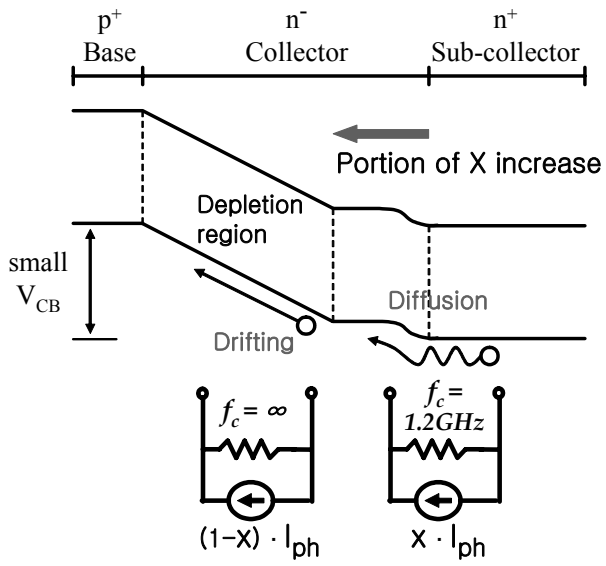

(a)

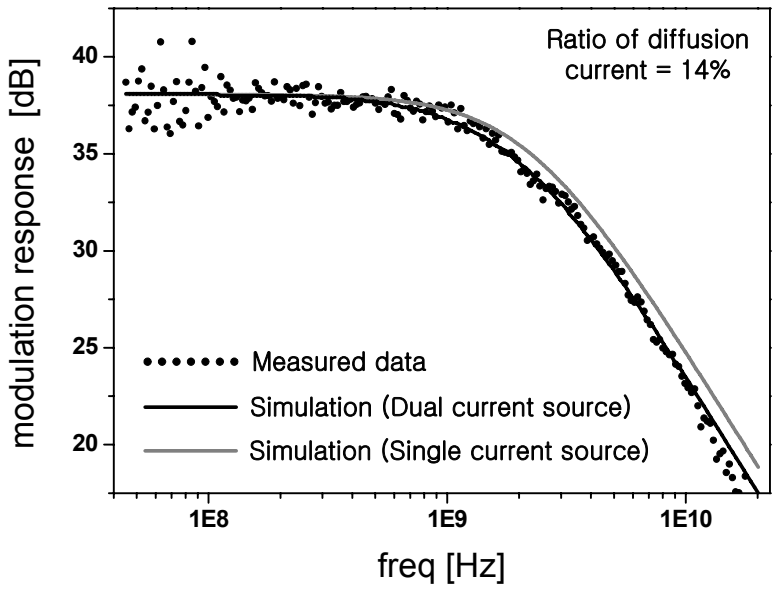

(b)

Figure 4.10 (a) Increasing of low-speed carrier where the small V_{CB} reduce the depletion region width. (b) Comparison of measured and simulated optical modulation response, where I_B and V_C are 400μA and 1V and input optical power is 0dBm.

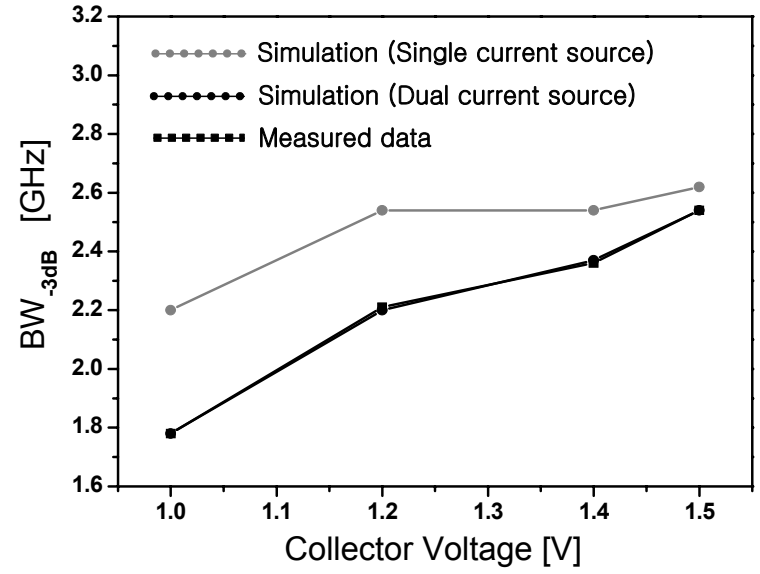

(a)

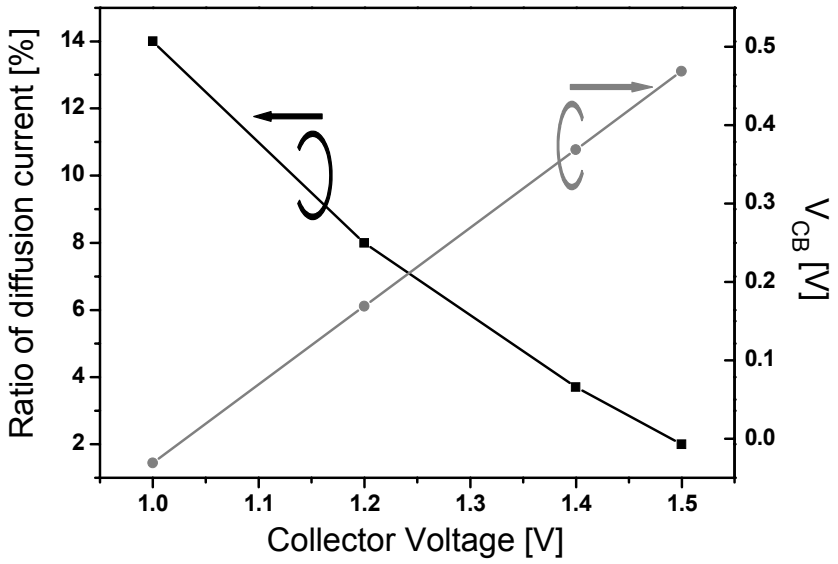

(b)

Figure 4.11 (a) 3dB bandwidth of measured and simulated optical modulation response (b) Diffusion current ratio and V_{CB} versus collector voltage, where I_B is 400μA and optical power is 0dBm.

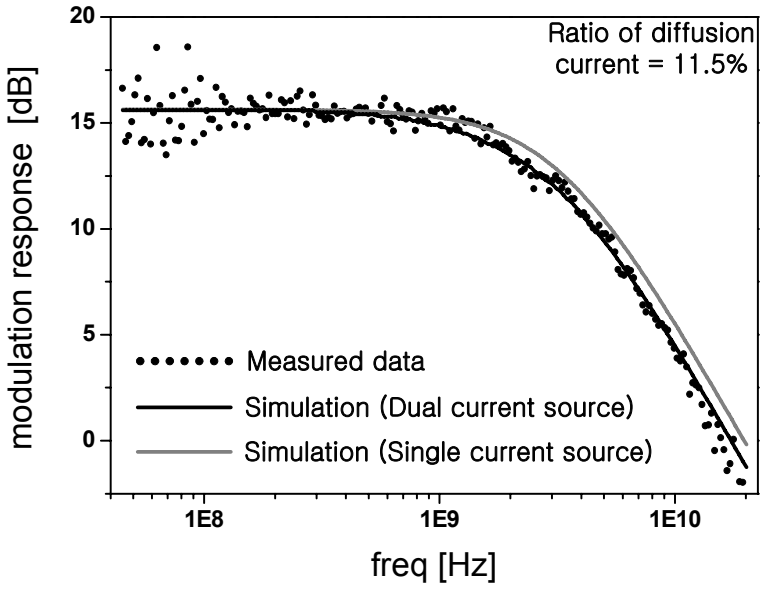

(a)

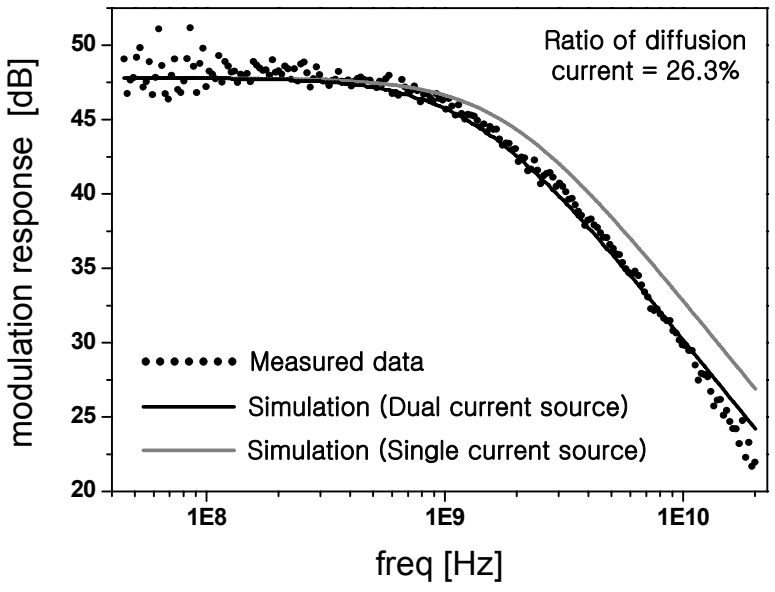

(b)

Figure 4.12 Fitting result of simulated photo-response on measured data using single and dual current source model, where I_B and V_C are 200㎂ and 1V and input optical power is (a) -9dBm (b) 4.8dBm.

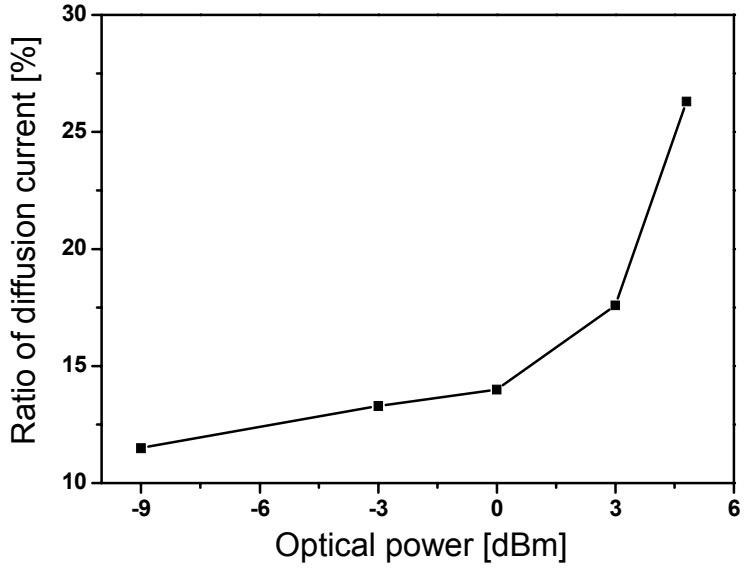

(a)

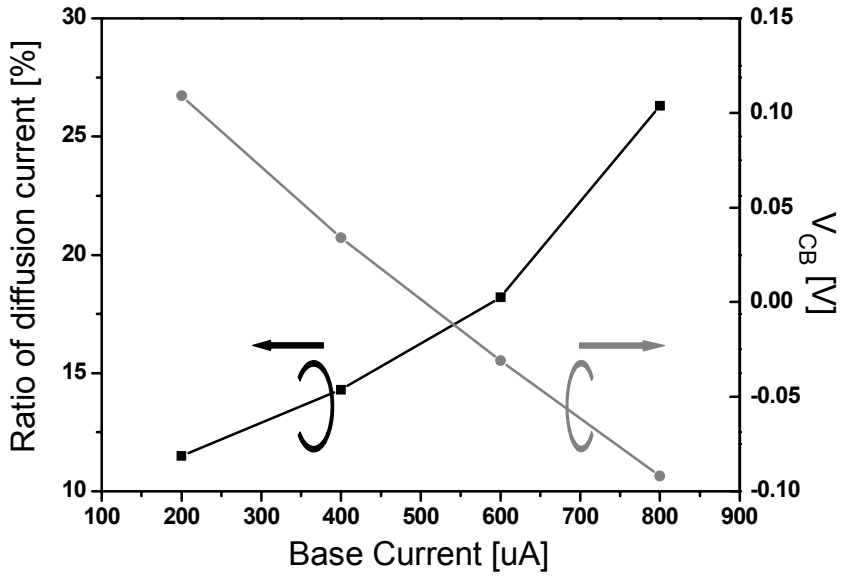

(b)

Figure 4.13 (a) Diffusion current ratio versus input optical power, where I_B and V_C are 200μA and 1V. (b) Diffusion current ratio and V_{CB} versus base current, where V_C is 1V and optical power is 0dBm.

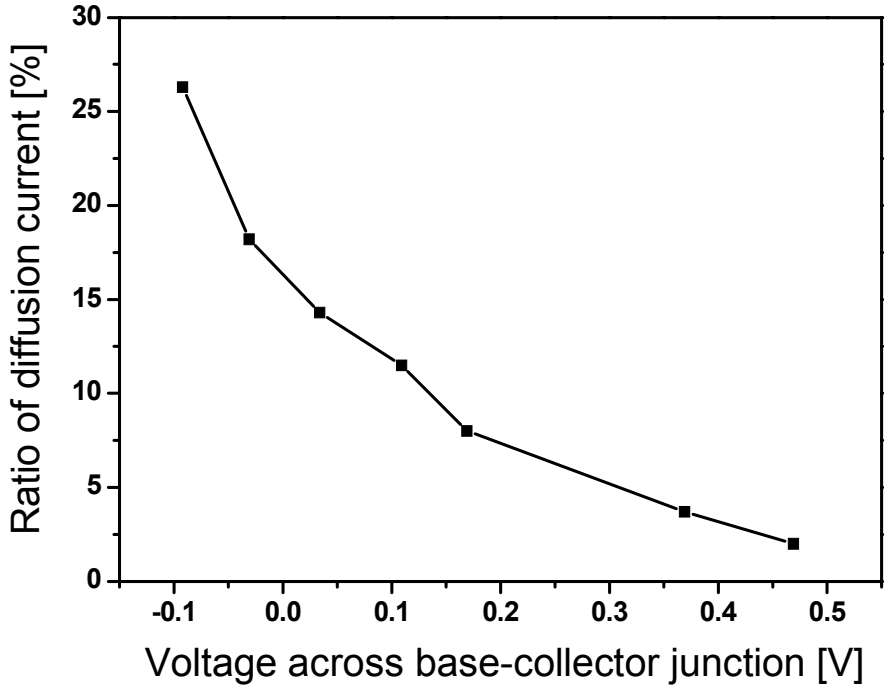

Figure 4.14 Relationship between the ratio of low-speed carrier and collector-base bias voltage. These relationships were extracted from several bias points where the optical modulation response was modeled.

Ⅴ. Large signal modeling

With previously developed DC equivalent circuit model and AC small-signal models according to DC bias points, AC large-signal operation of InP/InGaAs HPT was modeled as shown in Fig. 5.1. In large-signal model, DC components such as diodes and current gain are same with that of previously developed DC model, and the resistance values were obtained from AC small-signal model. The capacitive components were modeled by fixed capacitors or variable capacitors based on small-signal model parameters shown in chapter 3. The variable capacitors were modeled by equations which describe the dependence of capacitance values on DC bias condition. For describing AC photo-response of HPT, the large-signal AC photocurrent model was also developed and included in large-signal model.

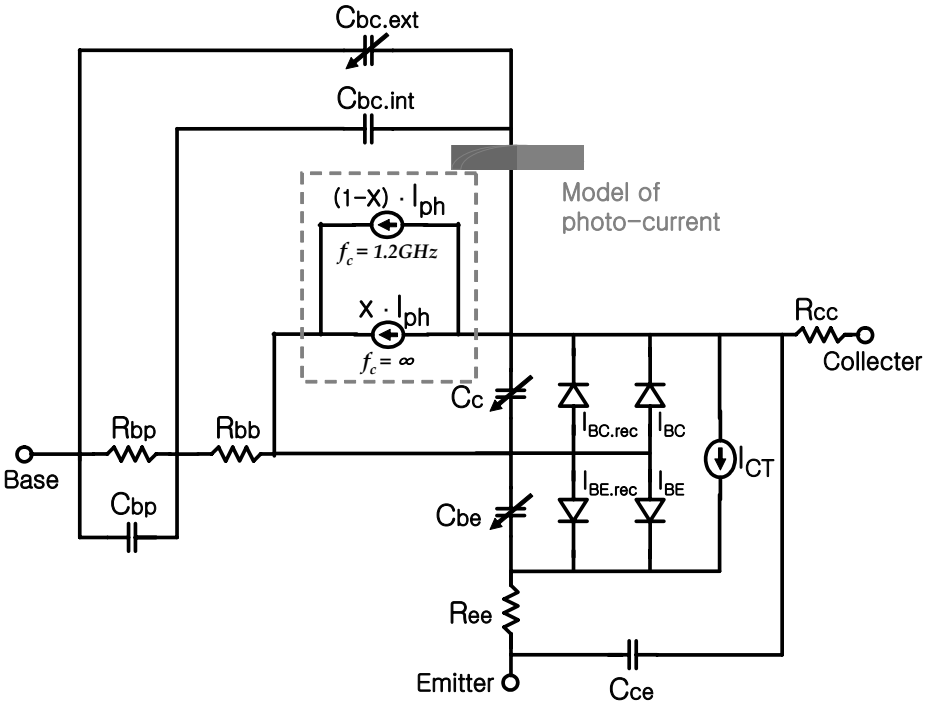

Figure 5.1 Large-signal equivalent circuit model. Parameters of diodes and Current gain were obtained from DC model. Capacitance and resistance values were obtained from AC small-signal models

A. Modeling of variable capacitors

Developed large-signal model has 3 variable capacitors such as C_{BE}, $C_{BC.EXT}$ and C_C. C_{BE} is dominantly depending on bias condition of base-emitter junction, and $C_{BC.EXT}$ and C_C are depending on bias condition of base-collector junction. These components were modeled by numerical equation that describes the effect of their dominant bias condition on each of them.

(A.1) Modeling of C_{BE}

C_{BE} represents the diffusion capacitance and junction capacitance of base-emitter junction. The value of this capacitance depends on the voltage across the junction [20]. As shown is Fig. 5.2, the C_{BE} which is obtained from small-signal model exponentially increases as voltage across the base-emitter junction. The values of voltage across the base-emitter junction are obtained from simulation using developed DC model. C_{BE} was modeled as variable capacitor of which value is a function of DC voltage across the capacitor, by numerical fitting of an exponential equation,

$$C_{BE} = (0.00005 \cdot e^{\frac{V_A}{0.0645}} + 44.9) \quad [fF] \qquad (5\text{-}1)$$

where

V_A voltage across the base-emitter junction.

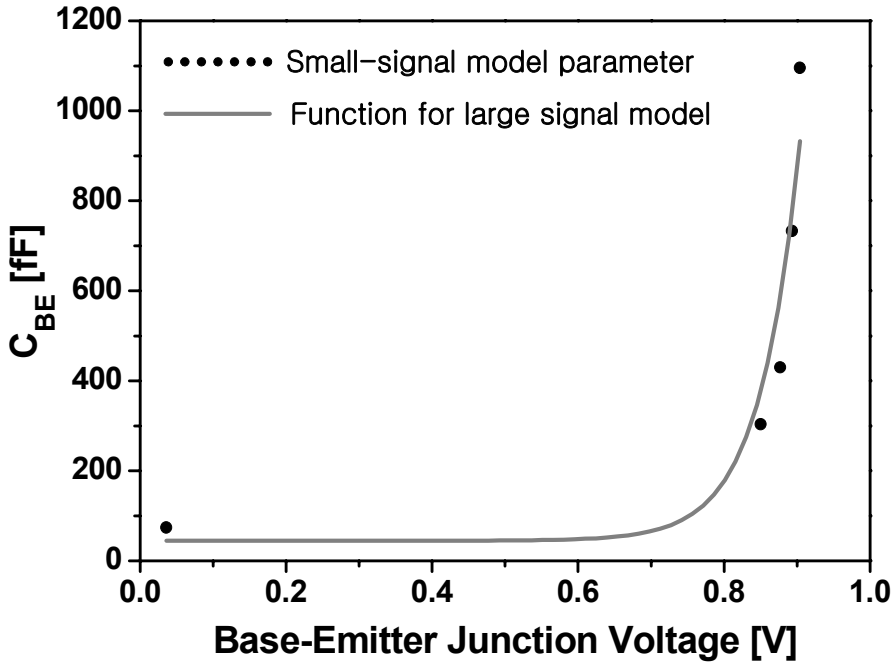

Figure 5.2 Comparison between C_{BE} on large-signal model and that of small-signal model versus base-emitter junction voltage.

(A.2) Modeling of $C_{BC.EXT}$, C_C

$C_{BC.EXT}$ and C_C are junction capacitances between base and collector region. The values of junction capacitance are mainly determined by width of depletion region. So, $C_{BC.EXT}$ and C_C can expressed as a function of voltage across base-collector junction [20]. Fig. 5.3 shows the values of $C_{BC.EXT}$ and C_C versus the base-collector junction voltage which was obtained from simulation using developed DC model. The large-signal models of $C_{BC.EXT}$ and C_C were obtained as functions of voltage across the capacitor by numerical fitting of the exponential equations,

$$C_{BC.EXT} = (6.4 \cdot e^{\frac{-V_A}{0.116}} + 15.2) \quad [fF] \tag{5-2}$$

$$C_C = (9.45 \cdot e^{\frac{-V_A}{0.155}} + 12.5) \quad [fF] \tag{5-3}$$

where

V_A voltage across the collector-base junction.

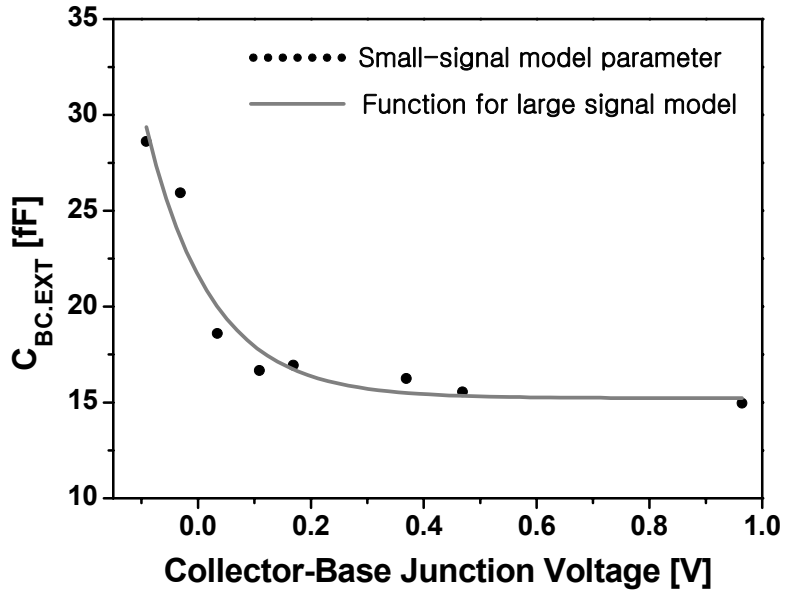

(a)

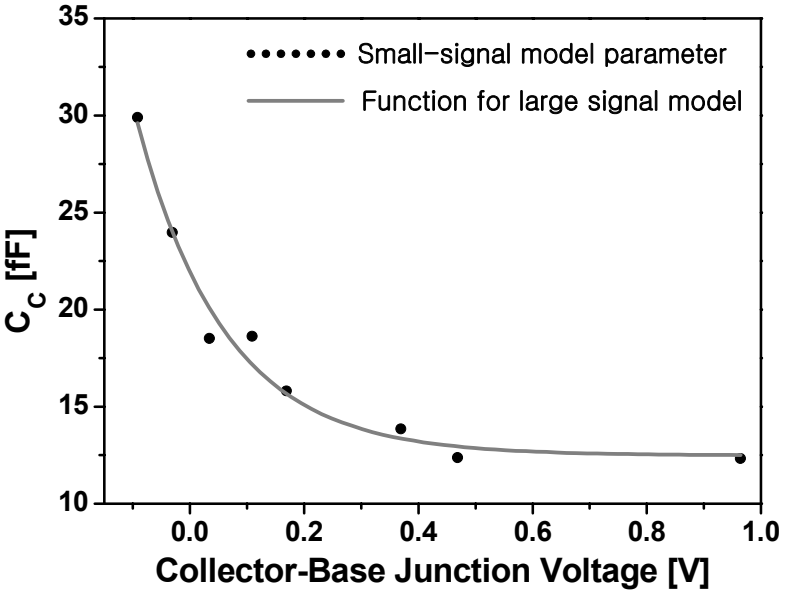

(a)

Figure 5.3 Comparison between large-signal model equation and small-signal model parameters of (a) $C_{BC.EXT}$ and (b) C_C.

B. Large-signal modeling of photocurrent

In large-signal model, optical illumination was described by dual current source photocurrent model which was mentioned in chapter 4. The ratio of diffusion current depends on DC bias voltage across collector-base junction in AC photocurrent model as shown in Fig. 5.4. So, the variable (x) representing the diffusion current ratio was inserted in large-signal model, where the value of the variable is a function of collector-base junction voltage,

$$X = \frac{1}{1 + e^{5.13 \cdot (V_A + 0.305)}} \tag{5-3}$$

where

V_A voltage across the collector-base junction.

This equation was obtained by numerical fitting of data shown in Fig. 5. 4. By the nature of this type of equation, the maximum value of X is 1, and minimum value is 0.

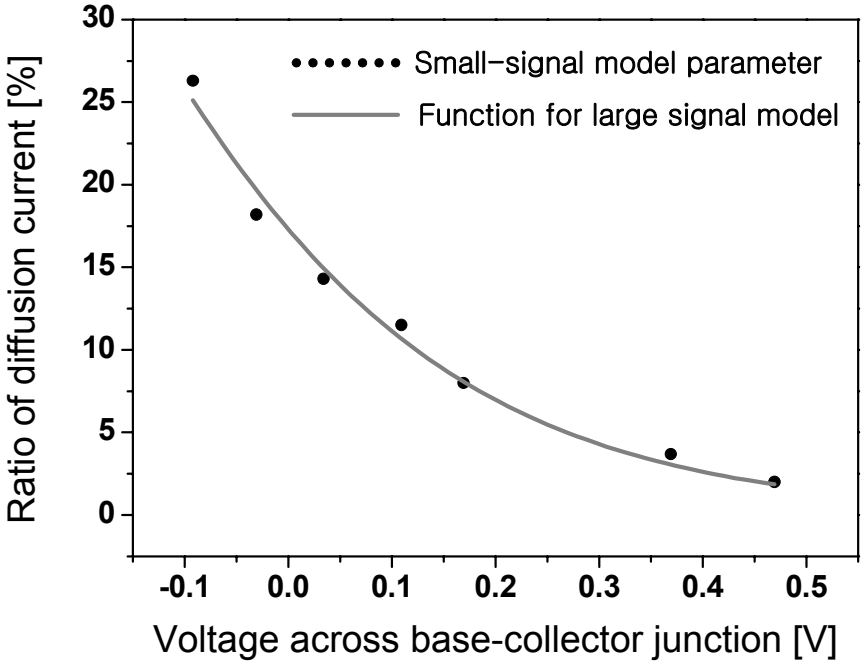

Figure 5.4 Comparison between large-signal model equation and small-signal model parameters for diffusion current ratio of photocurrent.

C. Verification of developed large-signal model

Using developed large signal model, optical modulation response and scattering response were simulated and compared with measured data. Fig. 5.5 shows comparison of simulated S-parameter and measured data, where I_B and V_C are 200μA and 1V and input optical power is 0dBm. The simulation result of large-signal model is similar with that of small-signal model. However, low frequency response of S_{21} is relatively high compare to the result using small-signal model. The reason is that the equivalent small-signal trans-conductance (gm_o) of developed DC model is larger than that of small-signal model. By the same reason, the simulated optical modulation response using large signal model exhibits relatively larger DC gain than simulation result using small-signal model as shown in Fig. 5.6.

To verify the large-signal description of developed model, the optoelectronic mixing characteristics of HPT were measured and compared to the simulated results using the model. As shown in Fig. 5.7, DFB laser diode (DFB LD) was directly modulated by 1GHz IF signal of which power is 15 dBm and generated optical signal was injected into the HPT through lensed fiber. The power of photo-detected IF signal was -28dBm when the HPT operated in PD-mode

(V_B=0V). On the other hand, the 10GHz LO signal was electrically injected into base terminal of HPT. Supplied LO power was -12dBm. The photo-detected IF signal was frequency up-converted into 9GHz and 11GHz bands by electrically supplied LO signal and nonlinear operation of HPT. Up-converted RF signal detected on collector port was measured with RF spectrum analyzer. Then, the conversion gain was obtained as a ratio of frequency up-converted RF power over photo-detected IF power at PD-mode operation of HPT,

$$Conversion\ gain = \frac{Up-converted\ RF\ \ power}{Detected\ IF\ \ power\ at\ PD-\mathrm{mod}e} \qquad (5\text{-}4)$$

The optoelectronic mixing characteristics were simulated using developed AC large-signal model. As a result, Fig 5.8 shows the spectrum of frequency up-converted RF signal, where I_B and V_C are 400μA and 1V, separately. The simulation results such as up-converted RF power and conversion gain are compared to the measured results over change of input optical power and collector bias voltage as shown in Fig. 5.9. The simulated and measured results have similar dependencies on input optical power and collector voltage. However, the simulated power of up-converted signal is relatively smaller than the measured one. It is because the photo-detected IF power in

simulation result is smaller than the measured one. In simulation result, the detected IF power was -47dBm in PD-mode operation, which is smaller than the measure result as much as 19dB. The cause of the difference was not found yet.

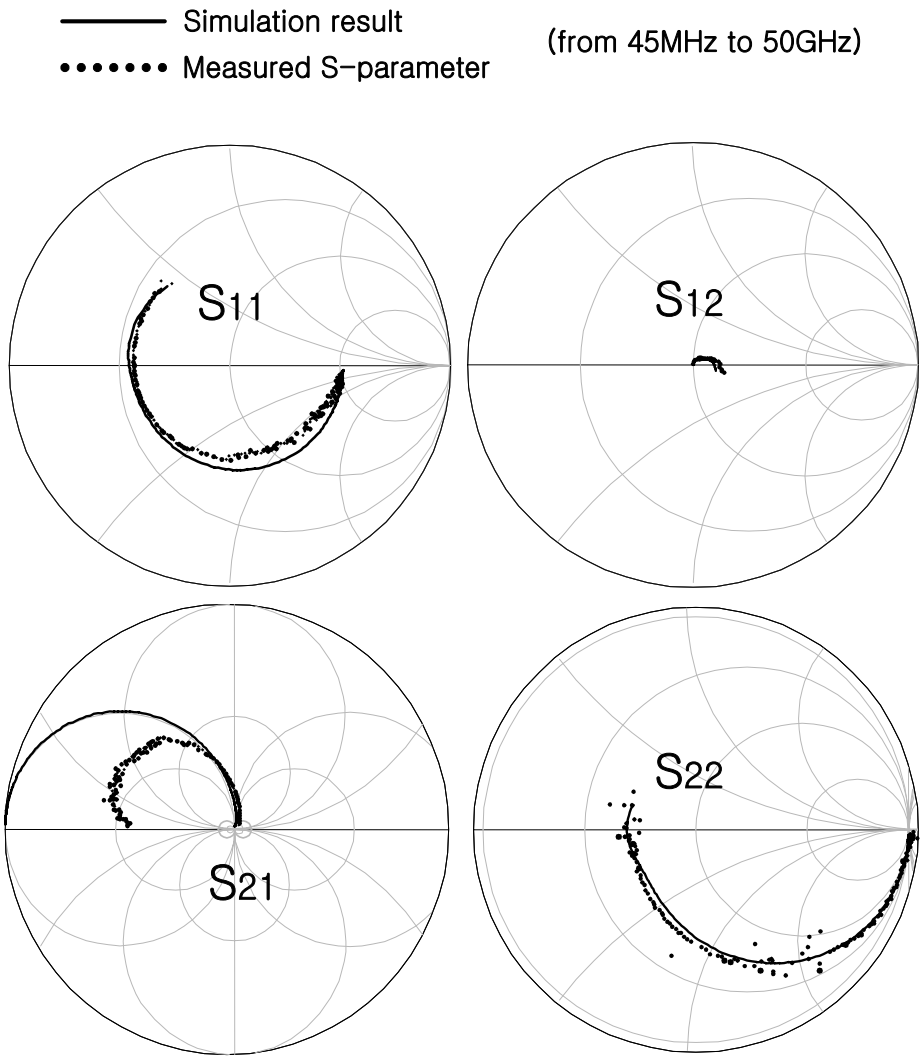

Figure 5.5 Comparison of simulated S-parameter using large-signal equivalent circuit model and measured data, where I_B and V_C are 200μA and 1V and input optical power is 0dBm.

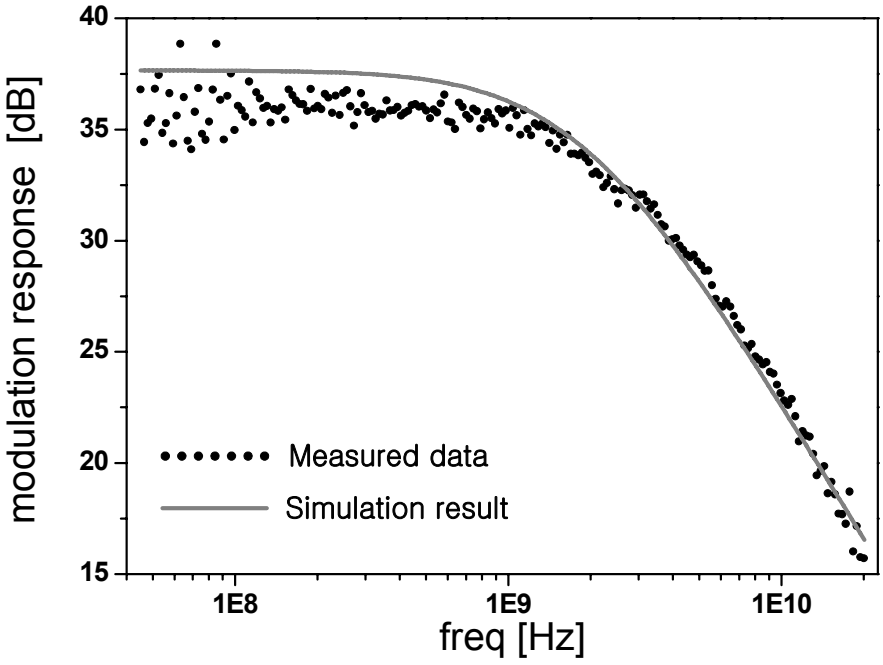

Figure 5.6 Comparison of simulated optical modulation response using large-signal equivalent circuit model and measured data, where I_B and V_C are 200μA and 1V and input optical power is 0dBm.

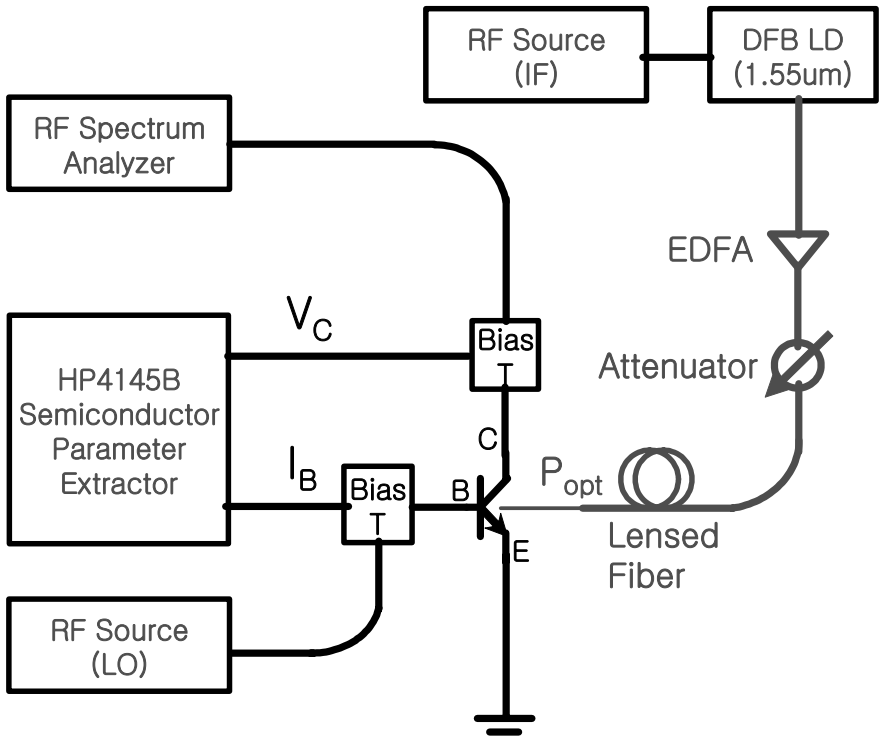

Figure 5.7 Measurement setup for optoelectronic mixing characteristics of InP/InGaAs HPT

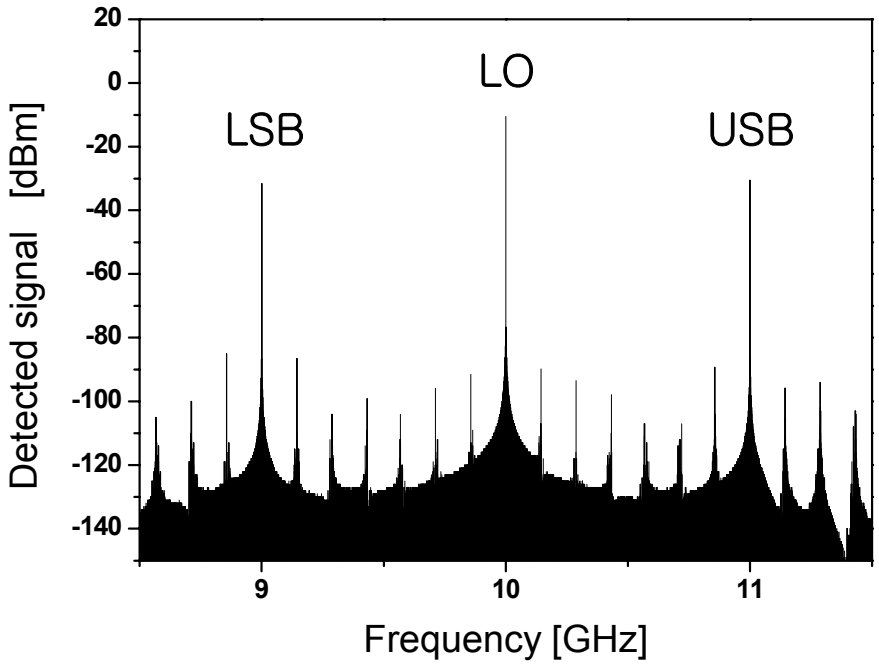

Figure 5.8 Spectrum of RF signals obtained from optoelectronic mixing simulation using large-signal equivalent circuit model, where I_B, V_C, input optical power and LO power are 400μA, 1V, 0dBm and -12dBm, separately.

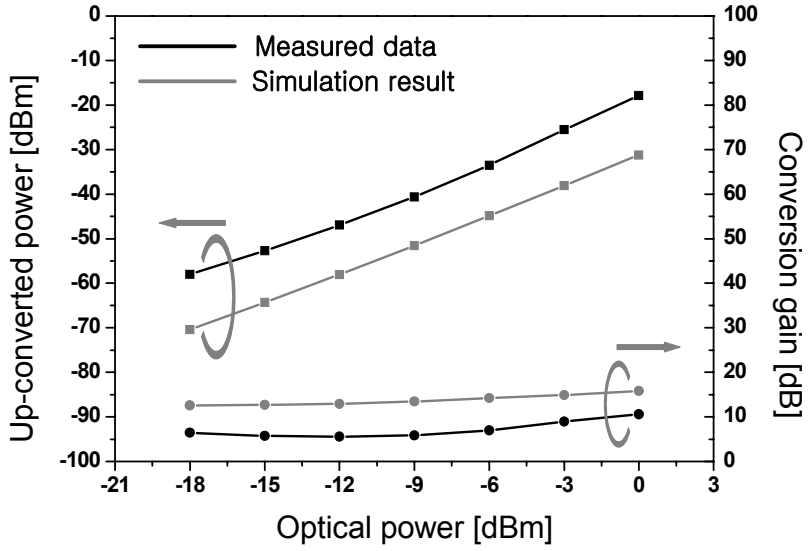

(a)

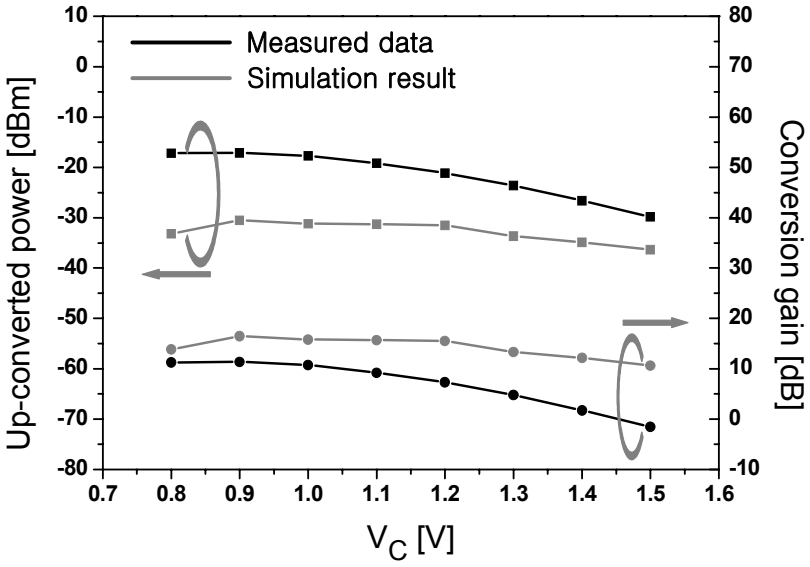

(b)

Figure 5.9 Measured and Simulated RF power and conversion gain of optoelectronic mixing (a) versus input optical power, where I_B, V_C and LO power are 400μA, 1V and -12dBm (b) versus collector voltage, where I_B, optical power and LO power are 400μA, 0dBm and -12dBm.

Ⅵ. Conclusion

Equivalent circuit model of InP/InGaAs HPT was developed focusing on the photo-detection characteristics. For describing of DC and AC photo-detection characteristics, optical illumination on HPT was modeled by adding DC and AC photocurrent model on electrical DC and AC small-signal models.

DC model of HPT was developed based on conventional Gummel-Poon equivalent circuit model. The electrical DC model parameters were extracted from Gummel-plots and open-collector and emitter methods. By adding simple DC photocurrent model, HPT model was accomplished and closely describes electrical DC characteristics of HPT under dark and optical illumination conditions. However, there is some discrepancy between DC characteristics of model and real device on high power optical illumination over 3dB. Further investigation about DC characteristic at high power optical illumination is needed.

AC small-signal model was developed as a hybrid-π type. Model parameters were extracted by numerical fitting of simulated S-parameters to measured data. Extracted model parameters show dependence on electrical and optical bias condition. For describing optical modulation response, dual current source model was employed

for photocurrent model. The dual current source model offers high accuracy by optimizing the ratio of diffusion current relating to bias condition.

The large-signal model was developed by combining the components of DC and AC models. Based on DC model, AC components such as variable capacitors and AC photocurrent model were supplemented. The developed large-signal model can describe not only DC and AC small-signal characteristics of HPT, but also large-signal characteristics such as optoelectronic mixing. In radio-on-fiber systems that use remote up-conversion scheme, the HPT optoelectronic mixer is very important part of antenna base stations. So, the developed HPT model can offer much advantage on design of radio-on-fiber systems. Moreover, each element included in this model basically own physical meaning, so that the developed model can support our analysis about the device operation.

However, the large signal model is less accurate than the individual DC and AC equivalent circuit model due to the discrepancy between equivalent trans-conductance on DC model and that on AC small-signal model. And the simulated photo-detection power of this model is relatively small compare to the measured result. Further investigation is needed for these problems.

References

[1] A. J. Seeds, “Microwave Photonics,” *IEEE Trans. Microwave Theory and Tech.*, Vol. 50, No. 3, pp. 877-887, March 2002

[2] G.. H. Smith and D. Novak, “Broadband millimeter-wave fiber-radio network incorporating remote up/downconversion,” *IEEE MTT-S International*, Vol. 3, pp. 1509 – 1512, June 1998

[3] J.M Fuster, J. Marti and J.L. Corral, “Chromatic dispersion effects in electro-optical up-converted millimetre-wave fibre optic links,” *Electronics Letters*, Vol. 33, Issue 23, pp.1969 – 1970, November 1997

[4] H. Kamitsuna, K. Ishii, T. Shibata, K. Kurishima and M. Ida, “A 43-Gb/s Clock and Data Recovery OEIC Integrating an InP-InGaAs HPT Oscillator with an HBT Decision Circuit,” *IEEE Journal of selected Topics in Quantum Electronics*, Vol. 10, No. 4, pp.673 – 678, July/August 2004

[5] C. S. Choi, J. Y. Kim, W. Y. Choi, H. Kamitsuna, M. Ida and K. Kurishima, “Optically Injection-Locked Self-Oscillating Optoelectronic Mixers Based on InP-InGaAs HPTs for Radio-on-Fiber Applications,” *IEEE Photonics Technology Letters*, Vol. 17, No. 11, pp.2415-2417, November 2005

[6] H. Kamitsuna, T. Shibata, K. Kurishima, and M. Ida, "Direct optical injection-locking of InP/InGaAs HPT oscillator ICs for microwave photonics and 40Gbit/s class optoelectronic clock recovery," *IEEE Trans. Microwave Theory and Tech.*, Vol. 50, No. 12, pp.3002-3008, December 2002

[7] Y. Betser, J. Lasri, V, Sidorov, S. Cohen, D. Ritter, M. Orentstein, G. Eisentstein, A. J. Seeds, A. Madjar, "An integrated heterojunction bipolar transistor cascode opto-electronic mixer," *IEEE Trans. Microwave Theory and Tech.*, Vol. 47, No. 7, pp. 1358-1364, July 1999

[8] O. Wada and H. Hasegawa, *InP-based Materials and Devices*, John Wiley & Sons, 1999

[9] K. Chang, I. Bahl and V. Nair, *RF and Microwave Circuit and Component Design for Wireless System*, John Wiley & Sons, 2002

[10] F. schwierz and J. J. Liou, *Modern Microwave Transistors*, John Wiley & Sons, 2003

[11] M. Ida, K. Kurishima, H. Nakajima, N, Watanabe and S. Yamahata, "Undoped-Emitter InP/InGaAs HBTs for High-Speed and Low-Power Applications," *IEEE International Electron Device Meeting*, pp.854-856, December 2000

[12] M. E. Hafizi, C. R. Crowell and M. E. Grupen, “The DC Characteristics of GaAs/AlGaAs Heterojunction Bipolar Transistors with Application to Device Modeling,” *IEEE Trans. on Electron Devices*, Vol. 37, No. 10, pp.2121-2129, October 1990

[13] Ke Lu, P. A Perry and T. J. Brazil, “A New Large-Signal AlGaAs/GaAs HBT Model Including Self-Heating Effects, with Corresponding Parameter-Extraction Procedure,” *IEEE Trans. Microwave Theory and Tech.*, Vol. 43, No. 7, pp.1433-1445, July 1995

[14] F. Sischka, “Gummel-poon toolkit B3_OHMIC.WPS| 19.12.01,” *Technical document of Agilent technology* (http://eesof.tm.agilent.com/docs/)

[15] S. M. Frimel and K. P. Roenker, “Gummel-Poon model for Npn heterojunction bipolar phototransistors,” *J. Appl. Phys.* pp.3581-3592, October 1997.

[16] D. Costa, W. U. Liu and J. S. Harris, “Direct Extraction of the AlGaAs/GaAs Heterojunction Bipolar Transistor Small-Signal Equivalent Circuit,” *IEEE Trans. on Electron Devices*, Vol. 38, No. 9, pp.2018-2024, September 1991.

[17] R. F. Pierret, *Semiconductor Device Fundamentals*, Addison-

Wesley, 1996

[18] J. Y. Kim, C. S. Choi, H. S. Kim, E. S. Nam and W. Y. Choi, "Equivalent circuit models for InP/InGaAs HPT," *Korea-Japan Joint Workshop on Microwave and Millimeter-wave Photonics*, pp. 91-94, January, 2005

[19] Hideki Kamitsuna, "Monolithic Optoelectronic Microwave /Millimeter-Wave Integrated Circuits Using Phototransistors," *Ph.D dissertation*, Graduate school of engineering, Kyushu University, Oct. 2004.

[20] Q. M. Zhang, H. Hu, J. Sitch, R. K. Surridge and J. M. Xu, "A new large signal HBT model," *IEEE Trans. Microwave Theory and Tech.*, Vol. 44, No. 11, pp.2001-2009, November 1996

국문요약

Radio-on-fiber 시스템을 위한 InP/InGaAs 이종접합 포토트랜지스터의 등가회로 모델링

본 논문에서는 InP/InGaAs 이종접합 포토트랜지스터의 등가회로 모델을 개발하였으며, Radio-on-fiber system에서의 응용을 위하여 포토트랜지스터의 광 검출 특성에 초점을 두었다.

DC 모델은 일반적인 Gummel-Poon 트랜지스터 모델을 기초로 하여 개발되었다. 측정된 Gummel plot으로부터 접합 다이오드들과 순방향 전류이득이 모델링 되었으며, 기생저항은 collector 개방 및 emitter 개방 측정을 이용하여 구해졌다. 간단한 구조의 DC 광 검출 전류 모델을 추가하여 완성된 DC모델은 이종접합 트랜지스터의 전기적, 광학적 특성을 매우 정확하게 묘사한다.

Hybrid-π 타입의 AC 소신호 등가회로는 측정된 S-parameter에 시뮬레이션 결과를 fitting 하는 방식으로 구해졌으며, 추출된 모델 parameter들은 전기적, 광학적

바이어스 조건에 대한 의존성을 보인다. AC 광 검출 특성을 묘사하기 위하여 AC 광 검출 전류 모델로 2개의 서로 다른 전류원을 사용하였으며, 이 중 확산전류의 비율은 base-collector 접합의 전압 차에 의해 결정된다. 개발된 AC 모델은 이종접합 포토트랜지스터의 AC 특성을 묘사함에 있어 높은 정확도를 보인다.

이종접합 포토트랜지스터의 대신호 등가회로는 DC 모델을 바탕으로, AC 소신호 등가회로에서 얻어진 구성요소들을 가변 콘덴서와 전류원 형태로 추가하여 구현되었다. 개발된 대신호 등가회로는 이종접합 포토트랜지스터의 전기적 및 광학적인 DC, AC 특성뿐만 아니라 광전 주파수 변환과 같은 대신호 특성을 모두 묘사할 수 있다. 또한 이 모델에 포함된 많은 회로 요소들은 각자 고유한 물리적 의미를 갖기 때문에, 개발된 등가회로는 소자의 동작 특성을 해석하는 것에도 많은 도움을 준다.